

1971

# Electron paramagnetic resonance studies and magnetic properties of low symmetry niobium(IV) complexes

William Ernst Antholine  
*Iowa State University*

Follow this and additional works at: <https://lib.dr.iastate.edu/rtd>

 Part of the [Physical Chemistry Commons](#)

## Recommended Citation

Antholine, William Ernst, "Electron paramagnetic resonance studies and magnetic properties of low symmetry niobium(IV) complexes" (1971). *Retrospective Theses and Dissertations*. 4936.  
<https://lib.dr.iastate.edu/rtd/4936>

This Dissertation is brought to you for free and open access by the Iowa State University Capstones, Theses and Dissertations at Iowa State University Digital Repository. It has been accepted for inclusion in Retrospective Theses and Dissertations by an authorized administrator of Iowa State University Digital Repository. For more information, please contact [digirep@iastate.edu](mailto:digirep@iastate.edu).

72-5171

ANTHOLINE, William Ernst, 1943-  
ELECTRON PARAMAGNETIC RESONANCE STUDIES AND  
MAGNETIC PROPERTIES OF LOW SYMMETRY NIOBIUM(IV)  
COMPLEXES.

Iowa State University, Ph.D., 1971  
Chemistry, physical

University Microfilms, A XEROX Company, Ann Arbor, Michigan

THIS DISSERTATION HAS BEEN MICROFILMED EXACTLY AS RECEIVED

Electron paramagnetic resonance studies and magnetic  
properties of low symmetry niobium(IV) complexes

by

William Ernst Antholine

A Dissertation Submitted to the  
Graduate Faculty in Partial Fulfillment of  
The Requirements for the Degree of  
DOCTOR OF PHILOSOPHY

Major Subject: Physical Chemistry

Approved:

Signature was redacted for privacy.

In Charge of ~~Major Work~~

Signature was redacted for privacy.

For the Major Department

Signature was redacted for privacy.

For the Graduate College

Iowa State University  
Ames, Iowa

1971

PLEASE NOTE:

Some Pages have indistinct  
print. Filmed as received.

UNIVERSITY MICROFILMS

## TABLE OF CONTENTS

	Page
INTRODUCTION	1
Review of Previous Niobium(IV) EPR Work	3
THEORETICAL	8
Introduction	8
Form of Potential for Quantization Along the $C_2$ Axis	12
Case I: Octahedral fields	12
Case II: Low symmetry ( $C_{2v}$ ) field	19
Effect of Crystal Field Potential on the d-Orbitals	20
Case I: Octahedral field	20
Case II: Octahedral field and spin orbit coupling	26
Low Symmetry Crystal Field Theory	30
g-Value Expressions	31
EXPERIMENTAL	38
Introduction	38
EPR spectrometer	38
Dewar and sample arrangements	38
Visible and infrared equipment	42
Crystals	42
EPR of $NbBr_4Ac_2$	46
Powder	46
Crystals	46
Glasses	57
Future work	62
Electronic Spectra of $NbBr_4Ac_2$	66
RESULTS AND DISCUSSION	73
Bonding	73
Magnetic Properties	81
BIBLIOGRAPHY	83
ACKNOWLEDGEMENTS	86

## INTRODUCTION

Several lower-valent metal halide complexes of the 4d transition metals in which two of the ligands in a six coordinate complex were either cis or trans i.e.  $MX_4L_2$  (M = metal, X = halide, L = cis or trans ligands) have been synthesized. These complexes have been characterized by ultraviolet, visible, and infrared spectroscopy, dipole moment measurements and powder magnetic susceptibility measurements which have indicated predominately cis rather than trans coordination. The magnetic properties have not been carefully studied; that is, susceptibility measurements have been taken only on powder samples at temperatures ranging from room temperature to 77°K. In some complexes the magnetic susceptibility has been measured only at room temperature.

The purpose of this investigation was to study in more detail the magnetic properties of a particular  $d^1$  complex using electron paramagnetic resonance as the diagnostic tool. The results then could be compared with powder magnetic susceptibility data to determine the extent one can rely on the susceptibility data to discriminate between cis and trans complexes. In addition, the EPR measurements were expected to provide information about the bonding of the complex

chosen. Theorists have not yet solved the exact eigenvalue problem for molecules as complicated as  $\text{MX}_4\text{L}_2$ . The goal of the author was to derive g-value expressions which agreed with experimental g-values. The goal was accomplished by splitting the d-orbitals with a low symmetry potential, formulating molecular orbital wave functions from the crystal field wave functions, and applying perturbation theory to account for the Zeeman splitting.

The particular complex chosen was tetrabromobis(acetonitrile)niobium(IV) where the niobium has the  $4d^1$  electron configuration. The preparation and characterization of this complex was reported by Torp (1). Therefore, details of the synthesis are not discussed in this thesis, and details of the characterization by susceptibility or electronic spectra were freely extracted from Torp's thesis. The X-ray structure determination of  $\text{NbBr}_4(\text{CH}_3\text{CN})_2$  reported by Dougherty (2) was the basis for the interpretation of EPR data for the  $\text{NbBr}_4(\text{CH}_3\text{CN})_2$  single crystals. Again, the details from the crystal structure determination were freely extracted from Dougherty's work.

## Review of Previous Niobium(IV) EPR Work

Few articles concerning electron paramagnetic resonance of niobium(IV) complexes have been reported since the initial work in the early and mid 1960's. The early Russian work stemmed from a 20-line EPR spectrum (ethanolic solution of niobium pentachloride and hydrogen chloride reduced by zinc) at 77°K obtained by Garif'yanov et al. (3). The spin Hamiltonian parameters were  $g_{\parallel}$  equal to 1.82,  $g_{\perp}$  equal to 1.80,  $A_{\parallel}$  equal to 270 gauss, and  $A_{\perp}$  equal to 146 gauss.

Following the Nb(IV) solution work, the Russians Vinokurov et al. (4) obtained EPR spectra of Nb(IV) impurities in natural single crystals of zircon,  $ZrSiO_4$ , and the next month Yafaev and Garif'yanov (5) reported the EPR spectrum of Nb(IV) in silicate glasses. The ten hyperfine lines observed from zircon at 77°K were attributed to Nb(IV) replacing Zr(IV) in a site surrounded by eight distorted oxygen nearest neighbors. The spin Hamiltonian parameters describing the ten line zircon spectra were  $g_{\parallel}$  equal to 1.862,  $g_{\perp}$  equal to 1.908,  $|A|$  equal to 309 Oe, and  $|B|$  equal to 138 Oe. The spin Hamiltonian parameters describing the EPR spectrum of Nb(IV) in silicate glasses at room temperature were  $g_{\parallel}$  equal to 1.89,  $g_{\perp}$  equal to 1.92,  $A$  equal to 310 Oe and  $B$  equal to 145 Oe. At 77°K



new lines were observed and attributed to Nb(IV) occupying two types of positions with different local electric fields due to "bridging" and "nonbridging" silicon-oxygen tetrahedra,  $\text{SiO}_4$ . The Nb(IV) ions were obtained by adding metallic aluminum and wood charcoal to the melt of silicate glasses of composition  $n\text{Na}_2\text{O} \cdot (98-n) \cdot \text{SiO}_2 \cdot 2\text{Nb}_2\text{O}_5$ .

Lardon and Günthard (6) reported an EPR spectrum of a Nb(IV) complex under conditions where they thought  $\text{NbCl}_6^{2-}$  ions should exist. The Nb(IV) complex was prepared by electrolytic reduction of  $\text{NbCl}_5$  in alcoholic solutions saturated with hydrogen chloride. The spin Hamiltonian parameters were  $g$  equal to 1.892 and  $A$  equal to 177.4 gauss for the Nb(IV) complex in a methanol solution at  $293^\circ\text{K}$ . The spin Hamiltonian parameters for the Nb(IV) complex in methanol, ethanol, and *i*-propanol glasses at  $77^\circ\text{K}$  varied slightly with a change in solvent. For the Nb(IV) complex in methanol  $g_1$  was equal to 1.892,  $g_3$  was equal to 1.925,  $A_1$  was equal to 131 gauss, and  $A_3$  was equal to 270 gauss. These glass spectra were fit assuming axial symmetry and a dependence of the half-width parameter on the orientation of the complex. Unfortunately, the formula of the species in solution was unknown and no chemical bonding interpretations were presented.

Rasmussen, Kuska, and Brubaker (7) reported the first EPR spectrum of a well characterized Nb(IV) complex, pentachloromethoxoniobate(IV) ion -  $\text{Nb}(\text{OCH}_3)\text{Cl}_5^{2-}$ . Assuming axial symmetry, the spin Hamiltonian parameters for the Nb(IV) complex in a methanol glass at 77°K were  $g_{\parallel}$  equal to 1.965,  $g_{\perp}$  equal to 1.809,  $|A| = 248$  gauss, and  $|B|$  equal to 144 gauss. The room temperature solution spectrum gave  $g$  equal to 1.861 and  $A$  equal to 178 gauss. Incorporating electronic spectra, an estimate for  $\langle r^{-3} \rangle$  for Nb(IV), and an estimate of  $\lambda$ , the spin-orbit coupling constant for Nb(IV), Brubaker suggested some rather covalent  $\sigma$  and  $\pi$  bonds.

Gainullin, Garif'yanov, and Kozyrev (8) synthesized  $\text{NbO}(\text{acac})_2$ ,  $\text{NbOCl}_4^{2-}$ , and  $\text{NbOF}_4^{2-}$ . The ESR parameters were typical for axially symmetric complexes. The parameters for  $\text{NbOCl}_4^{2-}$  were  $g_{\parallel}$  equal to 1.943,  $g_{\perp}$  equal to 1.932,  $A_{\parallel}$  equal to 260 gauss, and  $A_{\perp}$  equal to 122 gauss.

More recently (July 1969), Maniv, Low, and Gabay (9) reported EPR data on Nb(IV) in single crystals of  $\text{Cs}_2\text{ZrCl}_6$ . At 4.2°K and 80°K three EPR signals were observed for each orientation of the single crystal grown from the melt. Assuming tetragonal distortions along all three cubic axes, the spin Hamiltonian parameters were  $g_{\parallel}$  equal to 1.9184,  $g_{\perp}$

equal to 1.9515, A equal to 291.2 gauss, and B equal to 148.7 gauss.

Mackay and Schneider (10) published an interesting solution spectrum of  $(\text{Et}_4\text{N})_3(\text{Nb}_6\text{Cl}_{12})\text{Cl}_6$  consisting of 49 of the 55 hyperfine lines expected for a single electron delocalized over six niobium atoms. In other articles (11 through 16) spin Hamiltonian constants for the characteristic ten hyperfine lines due to the  $9/2$  spin of the niobium nucleus have been reported but the hyperfine coupling constants were an order of magnitude smaller than the hyperfine coupling constants for an electron in a predominately metal 4d-orbital and the g-values were often greater than the spin-only g-value.

As an example, Kim, Reardon, and Bray (14) observed a resolved spectrum from gamma-irradiated  $\text{Nb}_2\text{O}_5\text{-Na}_2\text{O-SiO}_2$  glass due to a Nb(IV) center and a tentative model of a hole in a  $\text{NbO}_6$  unit. The unresolved portion of the spectrum was attributed to a hole in a silicon-oxygen unit and to an electron captured at an oxygen vacancy in a silicon-oxygen unit. Spin Hamiltonian parameters for the  $d^1$  electron on the Nb(IV) center surrounded by six oxygens were  $g_{\parallel}$  equal to 1.8953,  $g_{\perp}$  equal to 1.9215, A equal to 325 gauss, and B equal to 164 gauss. Spin Hamiltonian parameters for the non- $d^1$  portion of

the spectrum were  $g$  approximately equal to 2.01 and  $A$  equal to 19.7 gauss.

This literature search thus resulted in a compilation of EPR spectra of Nb(IV) complexes. Reported  $g$ -values, coupling constants, and line shapes provided a basis to compare the experimental results with the EPR data from  $\text{NbBr}_4\text{Ac}_2$ . But, the theoretical expressions and experimental EPR data describing  $\text{NbBr}_4\text{Ac}_2$  were expected to be unique because the different ligands, bromide and acetonitrile, in the cis configuration added a low-symmetry potential. The standard expressions for octahedral and tetragonal symmetry no longer applied to the  $\text{NbBr}_4\text{Ac}_2$  complex. Therefore, a theoretical section for treating low-symmetry complexes precedes the discussion of experimental data.

## THEORETICAL

## Introduction

The axis of quantization for  $\text{NbBr}_4\text{Ac}_2$ , where Ac = acetonitrile, was the  $C_2$  axis in the point group  $C_{2v}$ . Many authors have treated low-symmetry complexes, but very few have attempted to adopt the axis of quantization shown in Fig. 1.

Bleaney, Bowers, and Pryce (17) have extended the theory developed by Abragam and Pryce (18) of paramagnetic resonance for the case of rhombic symmetry. A "mathematical" term,  $1/2 \sqrt{5} f(r)(ax^2+by^2+cz^2)$ , represented the ground state orbital wave function for a  $d^1$  Cu(II) complex with rhombic symmetry. Coupling constants for the magnetic hyperfine structure and g-values were expressed in terms of constants a, b, c, mixing parameters  $\alpha$ ,  $\beta$ ,  $\gamma$ , and spectroscopic splitting parameters u, v, w. Bleaney, Bowers, and Pryce (17) along with Sroubek and Zdansky (19) have compared this theory with experimental data for dilute crystals of Cu(II) complexes.

Ballhausen (20) gave the most "chemical" treatment for relative splittings of crystal field energy levels and g-value expressions for octahedral, tetragonal, and trigonal fields. Because symbolism was in terms of  $Dq$ ,  $Ds$ ,  $Dt$ ,  $e_g$ ,  $t_{2g}$ , etc. (chemical language), a procedure similar to

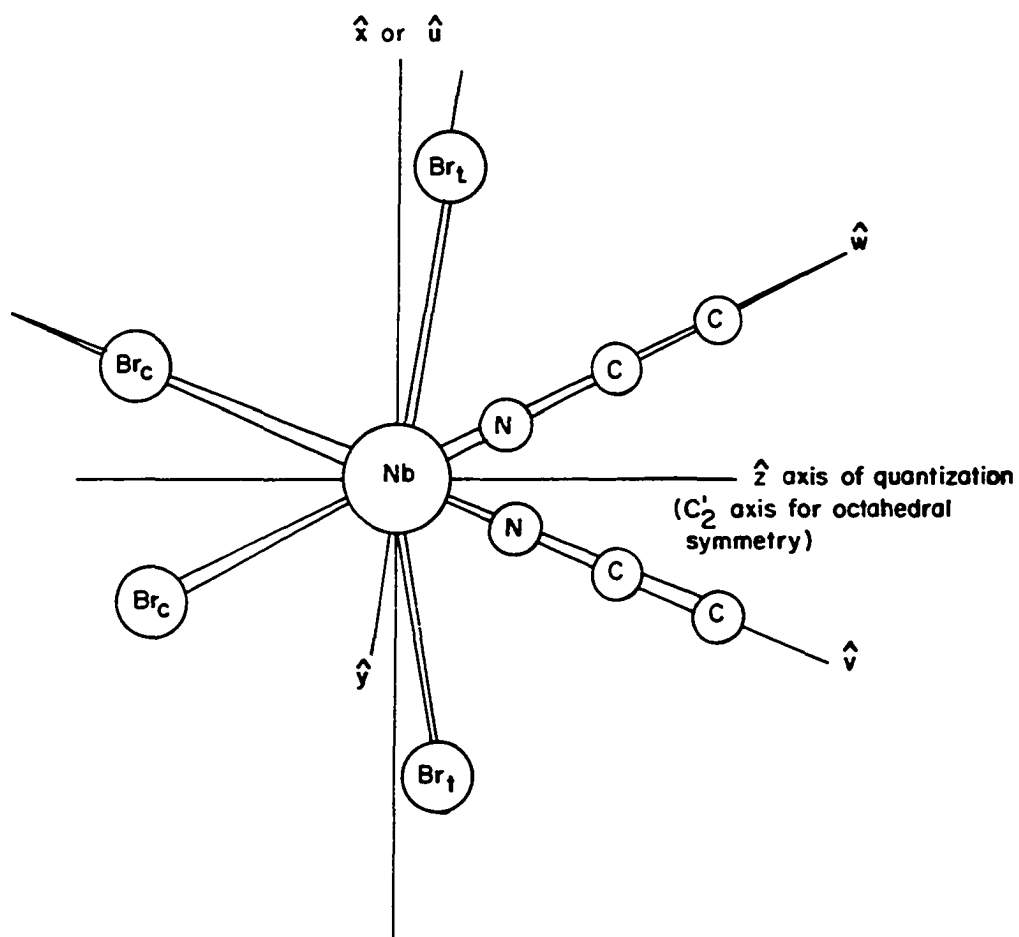


Fig. 1. The  $x$ ,  $y$ ,  $z$  principal axes and  $u$ ,  $v$ ,  $w$  bonding axes for  $\text{NbBr}_4(\text{CH}_3\text{CN})_2$

Ballhausen's treatment of  $d^1$  complexes with tetragonal or trigonal symmetry was used in this thesis to obtain expressions for the low symmetry crystal field potential and zero order wave functions with and without spin-orbit coupling.

Other authors have used the spatial wave functions of Ballhausen to explain their experimental results. Both Gladney and Swalen (21) ( $Ti^{3+}$  in trigonal environment) and Dionne (22) included interactions with the excited  $E_g$  states in deriving magnetic properties and crystal field parameters. Dionne's article treated  $D_{2h}$  symmetry where the axis of quantization was the same axis as the  $C_4$  axis in octahedral symmetry.

Starting with the d-orbital wave functions and g-value expressions for low-symmetry copper(II) complexes presented by McGarvey (23) Hitchman, Belford, et al. (24,25,26,27) in a series of articles interpreted the rhombic g-tensor for copper(II) and oxovanadium(IV) complexes. These authors were particularly concerned with rotation of the "in-plane" g-tensor (i.e.  $g_{xx}$  and  $g_{yy}$ ) and with the effect this rotation has on the ground state wave function. For this  $C_{2v}$  point group, where the x and y symmetry axes point along the ground state nodes, Hitchman (27) pointed out that the ground state

was the  $d_{xy}$  metal orbital and that no excited d-states were mixed into the ground state by the crystal field.

To a first approximation, the  $\text{NbBr}_4\text{Ac}_2$  complex was treated by crystal field theory - i.e. an "ionic" molecule in which the electron orbitals on the ligand were not allowed to overlap and mix with the electron orbitals on the metal ion. Therefore, the basic problem was to solve the Hamiltonian:

$$H = H_{\text{free ion}} + V_{\text{ligands}} .$$

Since solutions for the free ion were in terms of spherical harmonics, matrix elements for the potential  $V_L$ ,  $(\psi_i | V_L | \psi_j)$ , were easily obtained if the potential was expanded in terms of spherical harmonics. Because the Hamiltonian transforms as the totally symmetric representation, the potential must also transform as  $A_1$  under all operations of the symmetry group of the molecule. The spherical harmonic where  $l = 0$  uniformly shifts all energy levels. Since only relative energy levels may be measured, the  $l$  equal to zero spherical harmonic was neglected. For d electrons, spherical harmonics of odd order and spherical harmonics of order greater than four vanished due to the orthogonality and direct product relationships of the spherical harmonics. At this point



Ballhausen (20) treated the  $d^1$  problem in terms of tetragonal and trigonal splitting. In this thesis a similar outline for the  $d^1$  case is presented, where the axis of quantization for the d-orbitals is along the  $C_2$  axis of  $C_{2v}$  or along the  $C_2'$  axis of  $O_h$ .

### Form of Potential for Quantization Along the $C_2$ Axis

#### Case I: Octahedral fields

The assumption of an octahedral field seemed to be a crude approximation for  $NbBr_4Ac_2$ . Actually the splitting of the d-orbitals by an octahedral crystal field potential (splitting determined by the single parameter  $10 Dq$ ) was the predominate crystal field potential (see Fig. 2). Further splitting of the familiar  $t_{2g}$  and  $e_g$  orbitals by a low symmetry potential was less than 25% of  $10 Dq$ . So the procedure here was to calculate the octahedral potential and  $e_g$  and  $t_{2g}$  wave functions. Then these zero order wave functions were used to calculate g-value expressions from perturbation theory. Finally attempts were made to include the low symmetry crystal field potential and to refine the g-value expressions.

Only the  $Y_4^{m\ell}$  spherical harmonics had an  $A_{1g}$  irreducible component and only the  $Y_4^{m\ell}$  spherical harmonics were used for

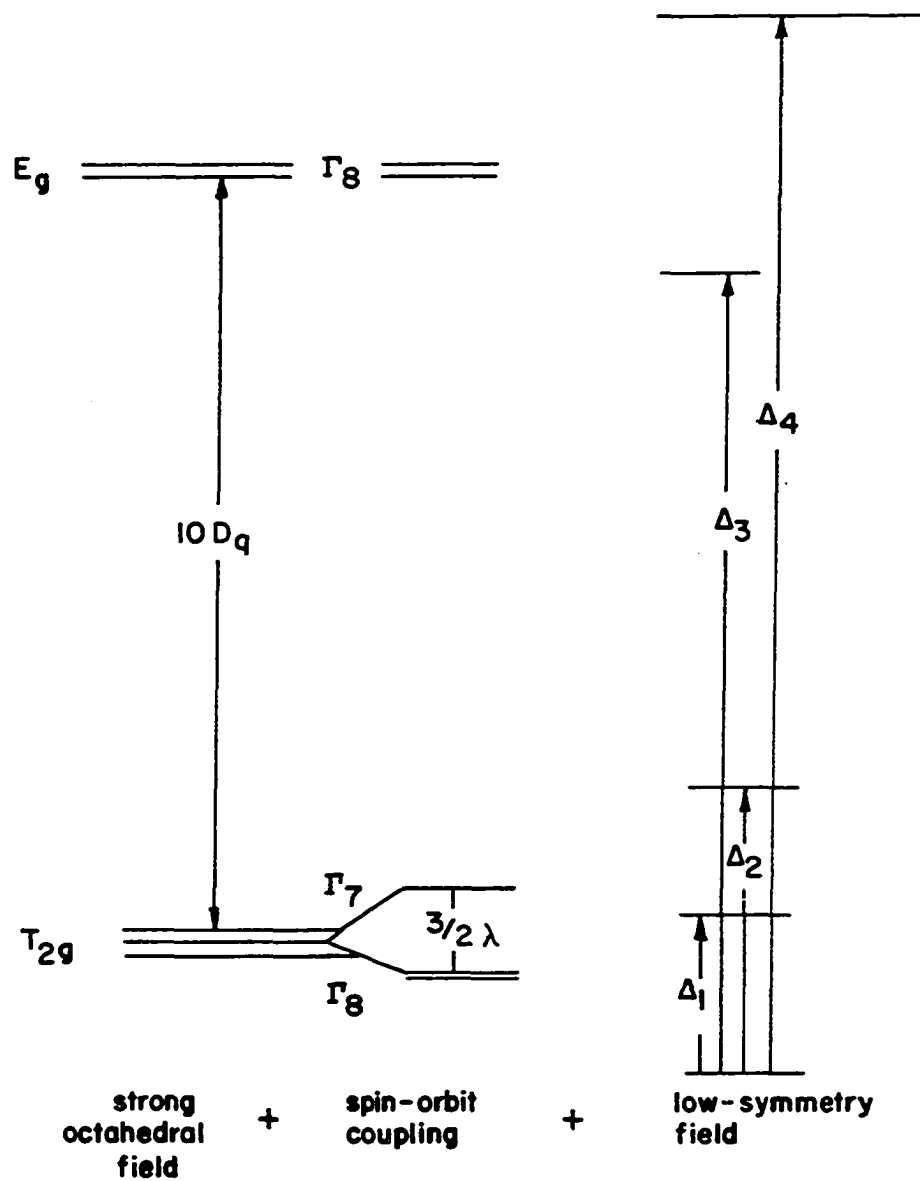


Fig. 2. The splitting of octahedral energy levels of the  $d'$  configuration with spin-orbit coupling and crystal field of  $C_{2v}$  symmetry

the expansion of the octahedral potential into a series of spherical harmonics. The  $C_2'$  axis for octahedral point symmetry was taken as the axis of quantization. Then  $C_2$ ,  $C_2'$ , and  $C_4$  symmetry operators rotated the coordinate system (Fig. 1) according to Equations 1-3.

$$C_2 \begin{vmatrix} x \\ y \\ z \end{vmatrix} = \begin{vmatrix} x \\ -y \\ -z \end{vmatrix} \quad (1)$$

$$C_2' \begin{vmatrix} x \\ y \\ z \end{vmatrix} = \begin{vmatrix} -x \\ -y \\ z \end{vmatrix} \quad (2)$$

$$C_4 \begin{vmatrix} x \\ y \\ z \end{vmatrix} = \begin{vmatrix} x \\ z \\ -y \end{vmatrix} \quad (3)$$

Operating with the  $C_2'$  symmetry operator on  $Y_4^{m\ell}$  gave:

$$C_2' \begin{vmatrix} Y_4^4 \\ Y_4^3 \\ Y_4^2 \\ Y_4^1 \\ Y_4^0 \\ Y_4^{-1} \\ Y_4^{-2} \\ Y_4^{-3} \\ Y_4^{-4} \end{vmatrix} = \begin{vmatrix} Y_4^4 \\ -Y_4^3 \\ Y_4^2 \\ -Y_4^1 \\ Y_4^0 \\ -Y_4^{-1} \\ Y_4^{-2} \\ -Y_4^{-3} \\ Y_4^{-4} \end{vmatrix} \quad (4)$$

Since the potential must have transformed as the totally symmetric group,  $A_{1g}$ , Equation 5 was used to simplify the octahedral potential (Equation 6).

$$C_2' V_{\text{oct}} = V_{\text{oct}} \quad (5)$$

$$V_{\text{oct}} = aY_4^0 + bY_4^2 + cY_4^{-2} + dY_4^4 + eY_4^{-4} \quad (6)$$

Operating with the  $C_2$  symmetry operator on the spherical harmonics for the simplified octahedral potential gave:

$$C_2 \begin{vmatrix} Y_4^0 \\ Y_4^2 \\ Y_4^{-2} \\ Y_4^4 \\ Y_4^{-4} \end{vmatrix} = \begin{vmatrix} Y_4^0 \\ Y_4^{-2} \\ Y_4^2 \\ Y_4^{-4} \\ Y_4^4 \end{vmatrix} \quad (7)$$

Again Equation 8 was used to simplify the potential (Equation 9 and Equation 10).

$$C_2 V_{\text{oct}} = V_{\text{oct}} \quad (8)$$

$$V_{\text{oct}} = aY_4^0 + b(Y_4^2 + Y_4^{-2}) + c(Y_4^4 + Y_4^{-4}) \quad (9)$$

$$V_{\text{oct}} = Y_4^0 + b(Y_4^2 + Y_4^{-2}) + c(Y_4^4 + Y_4^{-4}) \quad (10)$$

unnormalized

Operating with the  $C_4$  symmetry operator on the spherical harmonics for the unnormalized potential gave:

$$C_4 \begin{vmatrix} Y_4^0 \\ Y_4^2 + Y_4^{-2} \\ Y_4^4 + Y_4^{-4} \end{vmatrix} = C_4 \begin{vmatrix} \frac{1}{\sqrt{64}} & \frac{35z^2 - 30z^2r^2 + 3r^4}{r^4} \\ 2\sqrt{\frac{5}{32}} & \frac{(x^2 - y^2)(z^2 - r^2)}{r^4} \\ 2\sqrt{\frac{35}{128}} & \frac{x^4 - 6x^2y^2 + y^4}{r^4} \end{vmatrix} \quad (11)$$

$$= \begin{vmatrix} \frac{1}{\sqrt{64}} & \frac{35y^4 - 3y^2r^2 + 3r^4}{r^4} \\ 2\sqrt{\frac{5}{32}} & \frac{(x^2 - z^2)(y^2 - r^2)}{r^4} \\ 2\sqrt{\frac{35}{128}} & \frac{x^4 - 6x^2z^2 + z^4}{r^4} \end{vmatrix}$$

Again Equation 12 was used to collect terms in  $z^4$  (Equation 13).

$$C_4 V_{\text{oct}} = V_{\text{oct}} \quad (12)$$

$$c_2 \sqrt{\frac{35}{128}} + b_2 \sqrt{\frac{5}{32}} = \frac{5}{8} \quad (13)$$

Collecting terms in other variables did not give another independent equation. Therefore, the  $C_3$  rotation was considered where  $u$ ,  $v$ , and  $w$  are the bonding axes (Fig. 1).

$$\begin{vmatrix} u \\ v \\ w \end{vmatrix} = \begin{vmatrix} 1 & 0 & 0 \\ 0 & \frac{1}{\sqrt{2}} & \frac{1}{\sqrt{2}} \\ 0 & -\frac{1}{\sqrt{2}} & \frac{1}{\sqrt{2}} \end{vmatrix} \begin{vmatrix} x \\ y \\ z \end{vmatrix} \quad (14)$$

$$\begin{vmatrix} u' \\ v' \\ w' \end{vmatrix} = C_3 \begin{vmatrix} u \\ v \\ w \end{vmatrix} = \begin{vmatrix} 0 & 1 & 0 \\ 0 & 0 & 1 \\ 1 & 0 & 0 \end{vmatrix} \begin{vmatrix} u \\ v \\ w \end{vmatrix} = \begin{vmatrix} v \\ w \\ u \end{vmatrix} \quad (15)$$

$$C_3 \begin{vmatrix} x \\ y \\ z \end{vmatrix} = \begin{vmatrix} 1 & 0 & 0 \\ 0 & \frac{1}{\sqrt{2}} & -\frac{1}{\sqrt{2}} \\ 0 & \frac{1}{\sqrt{2}} & \frac{1}{\sqrt{2}} \end{vmatrix} \begin{vmatrix} 0 & 1 & 0 \\ 0 & 0 & 1 \\ 1 & 0 & 0 \end{vmatrix} \begin{vmatrix} x \\ y \\ z \end{vmatrix} = \begin{vmatrix} 1 & 0 & 0 \\ 0 & \frac{1}{\sqrt{2}} & \frac{1}{\sqrt{2}} \\ 0 & -\frac{1}{\sqrt{2}} & \frac{1}{\sqrt{2}} \end{vmatrix} \begin{vmatrix} x \\ y \\ z \end{vmatrix} \quad (16)$$

$$C_3 \begin{vmatrix} x \\ y \\ z \end{vmatrix} = \begin{vmatrix} 0 & \frac{1}{\sqrt{2}} & \frac{1}{\sqrt{2}} \\ -\frac{1}{\sqrt{2}} & -\frac{1}{2} & \frac{1}{2} \\ \frac{1}{\sqrt{2}} & -\frac{1}{2} & \frac{1}{2} \end{vmatrix} \begin{vmatrix} x \\ y \\ z \end{vmatrix} \quad (17)$$

Operating with the  $C_3$  symmetry operator on the spherical harmonics for the unnormalized potential gave:

$$C_3 \begin{vmatrix} Y_4^0 \\ Y_4^2 + Y_4^{-2} \\ Y_4^4 + Y_4^{-4} \end{vmatrix} = \frac{1}{\sqrt{64}} \frac{(35(\frac{x}{\sqrt{2}} - \frac{y+z}{2})^4 - 30(\frac{x}{\sqrt{2}} - \frac{y+z}{2})^2 r^2 + 3r^4)}{r^4} + \frac{2\sqrt{\frac{5}{32}}((\frac{y}{\sqrt{2}} - \frac{z}{\sqrt{2}})^2 - (-\frac{x}{\sqrt{2}} - \frac{y+z}{2})) (7(\frac{x}{\sqrt{2}} - \frac{y+z}{2})^2 - r^2)}{r^4} + \frac{2\sqrt{\frac{35}{128}}((\frac{y}{\sqrt{2}} + \frac{z}{\sqrt{2}})^4 - 6(\frac{y}{\sqrt{2}} + \frac{z}{\sqrt{2}})^2(-\frac{x}{\sqrt{2}} - \frac{y+z}{2})^2 + (-\frac{x}{\sqrt{2}} - \frac{y+z}{2})^4)}{r^4} \quad (18)$$

Again Equation 19 was used to collect terms in  $z^4$

(Equation 20),  $x^4$  (Equation 21), and  $y^4$  (Equation 22).

$$C_3 V_{\text{oct}} = V_{\text{oct}} \quad (19)$$

$$\sqrt{\frac{5}{32}} b - 14 \sqrt{\frac{35}{128}} c = \frac{165}{8} \quad (20)$$

$$-2 \sqrt{\frac{5}{32}} b - 6 \sqrt{\frac{35}{128}} c = \frac{25}{8} \quad (21)$$

$$-26 \sqrt{\frac{5}{32}} b - 46 \sqrt{\frac{35}{128}} c = \frac{85}{8} \quad (22)$$

Equation 22 was not independent of Equation 20 and Equation 21. Solving two equations in two unknowns yielded the constant,  $b$ , equal to  $\sqrt{10}$  and the constant  $c$  equal to  $-15/2 \sqrt{2/35}$ . The final form for the octahedral field, assuming the axis of quantization was  $C_2'$ , was:

$$V_{\text{oct}} = Y_4^0 + \sqrt{10}(Y_4^2 + Y_4^{-2}) - \frac{15}{2} \sqrt{\frac{2}{35}} (Y_4^4 + Y_4^{-4}) \quad (23)$$

### Case II: Low symmetry ( $C_{2v}$ ) field

In addition to the  $\ell = 4$  spherical harmonics, the  $\ell = 2$  spherical harmonics had a totally symmetric,  $A_1$ , irreducible component for  $C_{2v}$  point symmetry. Symmetry operations  $C_2$  and  $\sigma(xz)$  parameterized the potential into five terms:

$$V_{C_{2v}'} = aY_2^0 + b(Y_2^2 + Y_2^{-2}) + cY_4^0 + d(Y_4^2 + Y_4^{-2}) + e(Y_4^4 + Y_4^{-4}) \quad (24)$$



Unfortunately the potential expressed by Equation 24 seemed impractical to use because of the five unknown coefficients. This low symmetry potential did not leave enough degrees of freedom to determine coefficients to account for  $\pi$  and  $\sigma$  bonding or to calculate orbital reduction factors.

For the tetragonal case, Ballhausen (20) eliminated terms dependent on the  $x$  and  $y$  variables because the bonding was left unaltered in the  $xy$  plane due to substitution on the  $z$  axis. The bonding in the  $xy$  plane due to substitution in the  $yz$  plane was similarly unaltered for the cis complexes. Ballhausen (20) argued on the basis of a point charge model that the form of the potential for the cis and trans configuration was identical, but that the splitting due to the trans complex was twice the splitting of the cis complex. Also, the order for the energy terms for the cis and trans complexes were inverted. These arguments indicated that most of the perturbation of the octahedral potential by  $C_{2v}$  point symmetry was due to the  $Y_2^0$  and  $Y_4^0$  spherical harmonics.

#### Effect of Crystal Field Potential on the d-Orbitals

##### Case I: Octahedral field

Instead of solving the eigenvalue-eigenvector problem for  $d^1$  in an octahedral field, the transformation properties

of the d orbitals in an octahedral field were used to obtain linear combinations of the d-orbitals transforming as  $e_g$  and  $t_{2g}$ . That is, symmetry operations yielded wave functions for which the eigenvalue matrix was already diagonalized.

Using Ballhausen's (20) notation for treatment of tetragonal and trigonal symmetry, a d-orbital is expressed as a radial function  $R(r)$  times the spherical harmonic  $Y_2^{m_l}$  ( $d_{m_l} = Y_2^{m_l}$ ). The transformation properties of the d-orbitals in an octahedral field where the axis of quantization is the  $C_2'$  axis have been listed in Table 1.

Table 1. Transformation properties of d-orbitals in  $O_h$

E	$C_2'$	$C_2$	$C_4$	
				$z \rightarrow z$
	$x \rightarrow -x$	$y \rightarrow -y$	$y \rightarrow z$	
	$y \rightarrow -y$	$z \rightarrow -z$	$z \rightarrow -y$	
$d_2$	$d_2$	$d_2$	$d_{-2}$	$-\sqrt{\frac{3}{8}}d_0 + \frac{1}{4}(d_2+d_{-2}) - \frac{i}{2}(d_1-d_{-1})$
$d_1$	$d_1$	$-d_1$	$d_{-1}$	$\frac{1}{2}(d_2-d_{-2}) - \frac{1}{2}(d_1+d_{-1})$
$d_0$	$d_0$	$d_0$	$d_0$	$-\frac{1}{2}d_0 - \sqrt{\frac{3}{8}}(d_2+d_{-2})$
$d_{-1}$	$d_{-1}$	$-d_{-1}$	$d_1$	$-\frac{1}{2}(d_2-d_{-2}) - \frac{1}{2}(d_1+d_{-1})$
$d_{-2}$	$d_{-2}$	$d_{-2}$	$d_2$	$-\sqrt{\frac{3}{8}}d_0 + \frac{1}{4}(d_2+d_{-2}) + \frac{i}{2}(d_1-d_{-1})$
	$\chi(E) = 5$	$\chi(C_2') = 1$	$\chi(C_2) = +1$	$\chi(C_4) = -1$
$e_g$	2	0	2	0
$t_{2g}$	3	1	-1	-1

The d-orbitals were quantized along the  $C_2'$  axis when the  $C_2'$  symmetry operator operating on a d-orbital was equal to a constant times the same d-orbital (Equation 25).

$$C_2' d_{m_\ell} = (\text{constant})d_{m_\ell} \quad (25)$$

The transformation properties of the d-orbitals in Table 1 have already demonstrated that the d-orbitals have been quantized along the  $C_2'$  axis. If the constant for  $d_{m_\ell}$  after operating with the  $C_2'$  symmetry operator was equal to the constant for  $d_{m'_\ell}$ , a d-orbital with a different  $m_\ell$  value, the d-orbitals were allowed to mix (i.e. a linear combination of d-orbitals was a solution to the Schrödinger equation). From Table 1,  $d_2$ ,  $d_0$ ,  $d_{-2}$  did mix; similarly  $d_1$  and  $d_{-1}$  did mix.

The  $d_{yz}$  orbital was directed toward the cis bromides and the nitrogens from acetonitrile. Therefore,  $1/\sqrt{2}(d_1+d_{-1})$  was assumed to have been an  $e_g$  orbital. The linear combinations of d-orbitals for the  $e_g$  and  $t_{2g}$  orbitals were found by making use of symmetry operators and the characters for the  $T_{2g}$  and  $E_g$  representations as outlined below.

$$e_g^b = \frac{1}{\sqrt{2}}(d_1+d_{-1}) \quad (26)$$

$$e_g^a = ad_0 + bd_2 + cd_{-2} \quad (27)$$

$$C_2' e_g^a = e_g^a \quad (28)$$

$$C_2' e_g^b = -e_g^b \quad (29)$$

$$\chi(C_2') = 0 \quad (30)$$

The character for  $C_2'$  in the  $E_g$  representation, Equation 30, agreed with the sum of the characters for  $C_2'$  operating on the  $e_g^a$  and  $e_g^b$  orbitals (Equations 28 and 29).

$$C_2 e_g^a = C_2(ad_0 + bd_2 + cd_{-2}) = ad_0 + bd_{-2} + cd_2 \quad (31)$$

$$C_2 e_g^b = e_g^b \quad (32)$$

$$\chi(C_2) = 2 \quad (33)$$

The character for the  $C_2$  symmetry operator operating on the  $E_g$  representation was equal to two, the character for  $C_2$  operating on  $e_g^b$  was equal to plus one, therefore b and c were equal.

$$e_g^a = ad_0 + b(d_2 + d_{-2}) \quad (34)$$

$$e_g^b = \frac{1}{\sqrt{2}}(d_1 + d_{-1}) \quad (35)$$

$$C_4 e_g^a = a\left(-\frac{1}{2}d_0 - \sqrt{\frac{3}{8}}(d_2 + d_{-2})\right) + b\left(-\sqrt{\frac{3}{2}}d_0 + \frac{1}{2}(d_2 + d_{-2})\right) \quad (36)$$

$$C_4 e_g^b = -e_g^b \quad (37)$$

$$\chi(C_4) = 0 \quad (38)$$

The character for the  $C_4$  symmetry operator operating on

the  $E_g$  representation was equal to zero, the character for  $C_4$  operating on the  $e_g^b$  orbital was equal to minus one, therefore the character for  $C_4$  operating on the  $e_g^a$  orbital was equal to plus one as expressed in Equation 39.

$$\left(-\frac{a}{2} - \sqrt{\frac{3}{2}}b\right)d_0 + \left(\frac{b}{2} - \sqrt{\frac{3}{8}}a\right)(d_2+d_{-2}) = ad_0 + b(d_2+d_{-2}) \quad (39)$$

$$a = -\sqrt{\frac{2}{3}}b \quad (40)$$

$$e_g^a = -\frac{1}{2}d_0 + \sqrt{\frac{3}{8}}(d_2+d_{-2}) \quad (41)$$

$$e_g^b = \frac{1}{\sqrt{2}}(d_1+d_{-1}) \quad (42)$$

Since  $(d_2+d_{-2})$  mixed with  $d_0$  but not with  $(d_2-d_{-2})$  and  $(d_2-d_{-2})$  did not mix with  $d_0$  under the  $C_4$  symmetry operator,  $t_{2g}^a$  was set equal to a linear combination of  $d_0$  and  $(d_2+d_{-2})$ .

$$t_{2g}^a = ad_0 - b(d_2+d_{-2}) \quad (43)$$

The  $t_{2g}^a$  orbital orthogonal to the  $e_g^a$  orbital gave;

$$t_{2g}^a = -\frac{\sqrt{3}}{2}d_0 - \sqrt{\frac{1}{8}}(d_2+d_{-2}) \quad (44)$$

Since  $(d_1-d_{-1})$  was transformed into  $d_2-d_{-2}$  under the  $C_4$  symmetry operator;

$$t_{2g}^b = \frac{1}{\sqrt{2}}(d_1-d_{-1}) \quad (45)$$

$$t_{2g}^c = \frac{1}{\sqrt{2}}(d_2-d_{-2}) \quad (46)$$

The transformation properties and the representations for the zero order crystal field wave functions upon descent to  $C_{2v}$  symmetry have been summarized in Table 2.

Table 2. Transformation properties, wave functions, and representations upon descent to  $C_{2v}$  point symmetry for the d-orbital split by an octahedral field

	E	$C_2'$	$C_2$	$C_4$
$t_{2g}^a$	$t_{2g}^a$	$t_{2g}^a$	$t_{2g}^a$	$-t_{2g}^a$
$t_{2g}^b$	$t_{2g}^b$	$-t_{2g}^b$	$-t_{2g}^b$	$t_{2g}^c$
$t_{2g}^c$	$t_{2g}^c$	$t_{2g}^c$	$-t_{2g}^c$	$-it_{2g}^b$
$\chi(T_{2g})$	3	1	-1	-1
$e_g^a$	$e_g^a$	$e_g^a$	$e_g^a$	$e_g^a$
$e_g^b$	$e_g^b$	$-e_g^b$	$e_g^b$	$-e_g^b$
$\chi(E_g)$	2	0	2	0
$e_g^a = -\frac{1}{2} d_0 + \sqrt{\frac{3}{8}} (d_2 + d_{-2})$			$A_1$	Reduction to $C_{2v}$ point symmetry
$e_g^b = \frac{1}{\sqrt{2}} (d_1 + d_{-1})$			$B_2$	
$t_{2g}^a = -\frac{\sqrt{3}}{2} d_0 - \sqrt{\frac{1}{8}} (d_2 + d_{-2})$			$A_1$	
$t_{2g}^b = \frac{1}{\sqrt{2}} (d_1 - d_{-1})$			$B_1$	
$t_{2g}^c = \frac{1}{\sqrt{2}} (d_2 - d_{-2})$			$A_2$	

## Case II: Octahedral field and spin-orbit coupling

Niobium(IV) complexes have a large spin-orbit coupling constant  $\lambda$ . The number most quoted for  $\lambda$  has been  $748 \text{ cm}^{-1}$  obtained from Griffith (28). Therefore, the spin-orbit energy term was no longer small compared to the low-symmetry terms in the crystal field potential. The next step was to include spin-orbit coupling by calculating zero order wave functions with both spatial and spin functions. In octahedral symmetry, using the gamma notation of Bethe for the double group  $O_h'$  (20), the  $e_g$  functions transformed as  $\Gamma_8(^2E_g)$ , whereas the  $t_{2g}$  functions transformed as  $\Gamma_8(^2T_{2g})$  and  $\Gamma_7(^2T_{2g})$ . In Fig. 2 the octahedral energy levels of the  $d^1$  configuration were first split by spin-orbit coupling and then split by a crystal field potential to account for  $C_{2v}$  point symmetry.

Ballhausen investigated the  $t_{2g}$  and  $e_g$  functions with spin angular momentum and looked at the transformation properties of the  $t_{2g}$  and  $e_g$  wave functions to obtain  $\Gamma_8(^2T_{2g})$  and  $\Gamma_7(^2T_{2g})$ . This method used to obtain  $\Gamma_7(^2T_{2g})$  and  $\Gamma_8(^2T_{2g})$  when the axis of quantization was along the  $C_4$  symmetry axis was not adaptable to the  $e_g$  and  $t_{2g}$  functions when the axis of quantization was along the  $C_2'$  axis because of the complicated way the  $t_{2g}$  and  $e_g$  orbitals mix under spin-

orbit coupling. Without consideration of  $\Gamma_8(E_g)$  and  $\Gamma_8(T_{2g})$  interaction, solutions were obtained by solving the complete eigenvalue-eigenvector problem. The following Hamiltonian for spin-orbit coupling was considered:

$$H_\lambda = \lambda \mathbf{L} \cdot \mathbf{S} = \lambda (l_z s_z + \frac{1}{2} l^+ s^- + \frac{1}{2} l^- s^+) \quad (47)$$

where

$$l_+(l, m_l) = h \sqrt{(l+m_l+1)(l-m_l)} \quad (l, m_l+1) \quad (48)$$

$$l_-(l, m_l) = h \sqrt{(l-m_l+1)(l+m_l)} \quad (l, m_l-1) \quad (49)$$

The secular determinant was:

	$t_{2g^\alpha}^a$	$t_{2g^\beta}^b$	$t_{2g^\alpha}^c$	$t_{2g^\beta}^a$	$t_{2g^\alpha}^b$	$t_{2g^\beta}^c$
$t_{2g^\alpha}^a$	-E	$-\frac{\lambda}{2}$	$-\frac{\lambda}{2}$	0	0	0
$t_{2g^\beta}^b$	$-\frac{\lambda}{2}$	-E	$\frac{\lambda}{2}$	0	0	0
$t_{2g^\alpha}^c$	$-\frac{\lambda}{2}$	$\frac{\lambda}{2}$	-E	0	0	0
$t_{2g^\beta}^a$	0	0	0	-E	$\frac{\lambda}{2}$	$\frac{\lambda}{2}$
$t_{2g^\alpha}^b$	0	0	0	$\frac{\lambda}{2}$	-E	$\frac{\lambda}{2}$
$t_{2g^\beta}^c$	0	0	0	$\frac{\lambda}{2}$	$\frac{\lambda}{2}$	-E

The eigenvalues were  $\lambda$  and  $-\lambda/2$  as indicated in Fig. 2.

For the energy, E, equal to  $\lambda$ :



$$\Gamma_7^a(t_{2g}) = \sqrt{\frac{1}{3}} (t_{2g}^a{}^\alpha - t_{2g}^b{}^\beta - t_{2g}^c{}^\alpha) \quad (50)$$

$$\Gamma_7^b(t_{2g}) = \sqrt{\frac{1}{3}} (t_{2g}^a{}^\beta + t_{2g}^b{}^\alpha + t_{2g}^c{}^\beta) \quad (51)$$

For the energy, E, equal to minus  $\lambda/2$ , too few independent equations were obtained to determine the coefficients for the spin invested wave functions. For  $\Gamma_8^n(e_g)$ , where  $n = 1, 2, 3$  and 4, no levels were mixed implying:

$$\Gamma_8^1(e_g) = e_g^a{}^\alpha \quad (52)$$

$$\Gamma_8^2(e_g) = e_g^a{}^\beta \quad (53)$$

$$\Gamma_8^3(e_g) = e_g^b{}^\alpha \quad (54)$$

$$\Gamma_8^4(e_g) = e_g^b{}^\beta \quad (55)$$

The remaining problem was to determine the  $\Gamma_8^n(t_{2g})$  wave functions. The energy of the system had to be independent of the axis of quantization. From the octahedral case (treated by Ballhausen (20) with the  $C_4$  axis as the axis of quantization), the interaction of the  $\Gamma_8^n(e_g)$  and  $\Gamma_8^n(t_{2g})$  functions took the form:

$$\Gamma_8^n(e_g) = \lambda \sqrt{\frac{3}{2}} \Gamma_8^n(t_{2g}) \quad (56)$$

The wave functions were found from operating on  $\Gamma_8^n(e_g)$  functions having  $C_2$  axis as the axis of quantization with the

Hamiltonian,  $H_\lambda$ , and dividing by  $\lambda \sqrt{3/2}$ . In Table 3 the wave functions corresponding to the energy level diagram in Fig. 2 are listed.

Table 3. Zero order wave functions for  $\Gamma_8(^2E_g)$ ,  $\Gamma_7(^2T_{2g})$ , and  $\Gamma_8(^2T_{2g})$

---


$$\Gamma_8^1(e_g) = e_g^a \alpha$$

$$\Gamma_8^2(e_g) = e_g^a \beta$$

$$\Gamma_8^3(e_g) = e_g^b \alpha$$

$$\Gamma_8^4(e_g) = e_g^b \beta$$

$$\Gamma_7^a(t_{2g}) = \sqrt{\frac{1}{3}}(t_{2g}^a \alpha - t_{2g}^b \beta - t_{2g}^c \alpha)$$

$$\Gamma_7^b(t_{2g}) = \sqrt{\frac{1}{3}}(t_{2g}^a \beta + t_{2g}^b \alpha + t_{2g}^c \beta)$$

$$\Gamma_8^1(t_{2g}) = \frac{1}{\sqrt{2}}(-t_{2g}^b \beta + t_{2g}^c \alpha)$$

$$\Gamma_8^2(t_{2g}) = \frac{1}{\sqrt{2}}(t_{2g}^b \alpha - t_{2g}^c \beta)$$

$$\Gamma_8^3(t_{2g}) = \frac{1}{\sqrt{6}}(-2t_{2g}^a \beta + t_{2g}^b \alpha + t_{2g}^c \beta)$$

$$\Gamma_8^4(t_{2g}) = \frac{1}{\sqrt{6}}(-2t_{2g}^a \alpha - t_{2g}^b \beta - t_{2g}^c \alpha)$$


---

### Low Symmetry Crystal Field Theory

While zero order wave functions should give good estimates for the experimental g-values, no terms have yet been added to account for the low symmetry portion of the potential. The problem could be handled if the expression for the perturbation of the octahedral potential assumed the standard tetragonal form:

$$V_{C'_{2v}} = AR_2(r)Y_2^0 + BR_4(r)Y_4^0 \quad (57)$$

where A and B are constants and R is the radial part of the function. Using an operator technique and calling the radial integral for  $Y_2^0$ ,  $D_s$ , and for  $Y_4^0$ ,  $D_t$ , the following potential was obtained.

$$V_{C'_{2v}} = D_s(l^2 - 2) - D_t\left(\frac{35}{12}l^4 - \frac{155}{12}l^2 + 6\right) \quad (58)$$

The weak field matrix elements given below were useful in calculating strong field matrix elements for  $\Gamma_8(e_g)$ ,  $\Gamma_8(t_{2g})$ , and  $\Gamma_7(t_{2g})$  functions.

$$(d_{\pm 2} | V_{C'_{2v}} | d_{\pm 2}) = 2D_s - D_t \quad (59)$$

$$(d_{\pm 1} | V_{C'_{2v}} | d_{\pm 1}) = -D_s + 4D_t \quad (60)$$

$$(d_0 | V_{C'_{2v}} | d_0) = -2D_s - 6D_t \quad (61)$$

Matrix elements for the strong field without spin-orbit coupling were:

$$(e_g^a | V_{C_{2v}'} | e_g^a) = D_s - \frac{9}{4} D_t \quad (62)$$

$$(e_g^b | V_{C_{2v}'} | e_g^b) = -D_s + 4 D_t \quad (63)$$

$$(t_{2g}^a | V_{C_{2v}'} | t_{2g}^a) = -D_s - 4\frac{3}{4} D_t \quad (64)$$

$$(t_{2g}^b | V_{C_{2v}'} | t_{2g}^b) = -D_s + 4D_t \quad (65)$$

$$(t_{2g}^c | V_{C_{2v}'} | t_{2g}^c) = 2D_s - D_t \quad (66)$$

$$(t_{2g}^a | V_{C_{2v}'} | e_g^a) = -\sqrt{3} D_s - \frac{5\sqrt{3}}{4} D_t \quad (67)$$

Using these equations, the matrix elements for the strong field with spin-orbit coupling and with a low symmetry potential are presented in matrix form in Table 4.

#### g-Value Expressions

The spin-Hamiltonian formalism developed by Pryce (29) and used by Ballhausen (20) and Dionne (22) was accurate if  $\lambda$ , the spin-orbit coupling constant, was much smaller than the energy separation between the ground state and the first excited state. In the case of  $NbBr_4Ac_2$   $\lambda$  was probably about thirty per cent of this energy separation and the expressions for the g-values were not expected to be accurate. Perturba-

Table 4. Matrix elements for the strong field with spin-orbit coupling and with a low symmetry potential

	$\Gamma_8^1(t_{2g})$	$\Gamma_8^4(t_{2g})$	$\Gamma_7^a(t_{2g})$	$\Gamma_8^1(e_g)$	$\Gamma_8^4(e_g)$
$\Gamma_8^1(t_{2g})$	$(\frac{1}{2}D_s + \frac{3}{2}D_t)$ $-4D_q - \frac{\lambda}{2}$	$(-\frac{3}{\sqrt{12}}D_s + \frac{5}{\sqrt{12}}D_t)$	$(-\frac{3}{\sqrt{6}}D_s + \frac{5}{\sqrt{6}}D_t)$	$(-\sqrt{\frac{3}{2}}D_s - \frac{5}{4}\sqrt{\frac{3}{2}}D_t)$ $\sqrt{\frac{3}{2}}\lambda$	
$\Gamma_8^4(t_{2g})$	$(-\frac{3}{12}D_s + \frac{5}{12}D_t)$	$(-\frac{1}{2}D_s - \frac{8}{3}D_t)$ $-4D_q - \frac{\lambda}{2}$	$(\frac{1}{\sqrt{2}}D_s + \frac{25}{6\sqrt{2}}D_t)$	$(\frac{1}{\sqrt{2}}D_s + \frac{5}{4\sqrt{2}}D_t)$	$(\sqrt{\frac{3}{2}}\lambda)$
$\Gamma_7^a(t_{2g})$	$(-\frac{3}{\sqrt{6}}D_s + \frac{5}{\sqrt{6}}D_t)$	$(\frac{1}{\sqrt{2}}D_s + \frac{25}{6\sqrt{2}}D_t)$	$(-\frac{7}{12}D_t)$ $-4D_q + \lambda$	$(D_s + \frac{5}{4}D_t)$	
$\Gamma_8^1(e_g)$	$(-\sqrt{\frac{3}{2}}D_s - \frac{5}{4}\sqrt{\frac{3}{2}}D_t)$ $\sqrt{\frac{3}{2}}\lambda$	$(\frac{1}{\sqrt{2}}D_s + \frac{5}{4\sqrt{2}}D_t)$	$(D_s + \frac{5}{4}D_t)$	$(D_s - \frac{9}{4}D_t)$ $6D_q$	

Table 4. (Continued)

	$\Gamma_8^1(t_{2g})$	$\Gamma_8^4(t_{2g})$	$\Gamma_7^a(t_{2g})$	$\Gamma_8^1(e_g)$	$\Gamma_8^4(e_g)$
$\Gamma_8^4(e_g)$		$(\sqrt{\frac{3}{2}} \lambda)$			$(-D_s + 4D_t + 6D_q)$
	$\Gamma_8^2(t_{2g})$	$\Gamma_8^3(t_{2g})$	$\Gamma_7^b(t_{2g})$	$\Gamma_8^2(e_g)$	$\Gamma_8^3(e_g)$
$\Gamma_8^2(t_{2g})$	$(\frac{1}{2}D_s + \frac{3}{2}D_t - 4D_q - \frac{\lambda}{2})$	$(-\frac{3}{\sqrt{12}}D_s + \frac{5}{\sqrt{12}}D_t)$	$(-\frac{3}{\sqrt{6}}D_s + \frac{5}{\sqrt{6}}D_t)$	$(\sqrt{\frac{3}{2}}D_s + \frac{5}{4}\sqrt{\frac{3}{2}}D_t + \sqrt{\frac{3}{2}}\lambda)$	
$\Gamma_8^3(t_{2g})$	$(-\frac{3}{\sqrt{12}}D_s + \frac{5}{\sqrt{12}}D_t)$	$(-\frac{1}{2}D_s - \frac{8}{3}D_t - 4D_q - \frac{\lambda}{2})$	$(\frac{1}{\sqrt{2}}D_s + \frac{25}{6\sqrt{2}}D_t)$	$(-\frac{1}{\sqrt{2}}D_s - \frac{5}{4\sqrt{2}}D_t)$	$(\sqrt{\frac{3}{2}} \lambda)$

Table 4. (Continued)

	$\Gamma_8^2(t_{2g})$	$\Gamma_8^3(t_{2g})$	$\Gamma_7^b(t_{2g})$	$\Gamma_8^2(e_g)$	$\Gamma_8^3(e_g)$
$\Gamma_7^b(t_{2g})$	$(-\frac{3}{6}D_s + \frac{5}{6}D_t)$	$(-\frac{1}{2}D_s + \frac{25}{6 \cdot 2}D_t)$	$(-\frac{7}{12}D_t$ $-4D_q + \lambda)$	$(-D_s - \frac{5}{4}D_t)$	
$\Gamma_8^2(e_g)$	$(\sqrt{\frac{3}{2}}D_s + \frac{5}{4}\sqrt{\frac{3}{2}}D_t$ $\sqrt{\frac{3}{2}}\lambda)$	$(-\frac{1}{\sqrt{2}}D_s - \frac{5}{4\sqrt{2}}D_t)$	$(-D_s - \frac{5}{4}D_t)$	$(D_s - \frac{9}{4}D_t$ $6D_q)$	
$\Gamma_8^3(e_g)$		$(\sqrt{\frac{3}{2}}\lambda)$			$(-D_s + 4D_t$ $6D_q)$

tion theory developed by Pryce (29) gave an expression (Equation 68) for the anisotropic g-values

$$g_{ij} = 2(\delta_{ij} - \lambda \Lambda_{ij}) \quad (68)$$

where

$$\Lambda_{ij} = \sum_{n \neq \text{ground state}} \frac{(\text{ground state} | L_i | n) (n | L_j | \text{ground state})}{E_n - E_{\text{ground state}}} \quad (69)$$

and where i and j refer to x, y, z coordinate system in Fig. 1 and where n refers to the nth excited state. The following g-value expressions were obtained assuming the ground state transformed as a non-bonding  $A_2$  state (see Table 2).

$$g_{zz} = 2 \left( 1 - \frac{3\lambda}{E_{e_g^a} - E_{t_{2g}^c}} - \frac{\lambda}{E_{t_{2g}^a} - E_{t_{2g}^c}} \right) \quad (70)$$

$$g_{yy} = 2 \left( 1 - \frac{\lambda}{E_{t_{2g}^b} - E_{t_{2g}^c}} \right) \quad (71)$$

$$g_{xx} = 2 \left( 1 - \frac{\lambda}{E_{e_g^b} - E_{t_{2g}^c}} \right) \quad (72)$$

More accurate g-value expressions were obtained when the spin orbit coupling ( $\lambda L \cdot S$ ) and the Zeeman splitting ( $\beta H \cdot (L + 2S)$ ) were treated separately. If  $\lambda$ , the spin-orbit



coupling constant, was less than the separation between the ground state and the first excited state, the ground state wave function, as developed by Pake (30) and used by Dionne (22) was:

$$\psi_{m'} = \psi_m - \sum_{k \neq m} \psi_k \frac{\langle k | \lambda L \cdot S / m \rangle}{E_k - E_m} \quad (73)$$

Using the  $e_g$  and  $t_{2g}$  wave functions given in Table 2 and again assuming the ground state transformed as  $A_2$  gave:

$$t_{2g\alpha}^c = t_{2g\alpha}^c + \frac{\frac{\lambda}{2} t_{2g\alpha}^a}{E(t_{2g\alpha}^a) - E(t_{2g\alpha}^c)} - \frac{\frac{\lambda}{2} t_{2g\beta}^b}{E(t_{2g\beta}^b) - E(t_{2g\alpha}^c)} \quad (74)$$

$$+ \frac{\frac{\lambda}{2} e_{g\beta}^b}{E(e_{g\beta}^b) - E(t_{2g\alpha}^c)} - \frac{\frac{\sqrt{3}}{2} \lambda e_{g\alpha}^a}{E(e_{g\alpha}^a) - E(t_{2g\alpha}^c)}$$

$$t_{2g\beta}^c = t_{2g\beta}^c - \frac{\frac{\lambda}{2} t_{2g\beta}^a}{E(t_{2g\beta}^a) - E(t_{2g\beta}^c)} - \frac{\frac{\lambda}{2} t_{2g\alpha}^b}{E(t_{2g\alpha}^b) - E(t_{2g\beta}^c)} \quad (75)$$

$$- \frac{\frac{\lambda}{2} e_{g\alpha}^b}{E(e_{g\alpha}^b) - E(t_{2g\beta}^c)} + \frac{\frac{\sqrt{3}}{2} \lambda e_{g\beta}^a}{E(e_{g\beta}^a) - E(t_{2g\beta}^c)}$$

The Zeeman energy split the  $\psi_{t_{2g\alpha}}$  and  $\psi_{t_{2g\beta}}$  ground state doublet. Matrix elements were calculated for the Zeeman splitting using Equation 76.

$$H_{ij} = (\psi_i | \beta H(L+2S) | \psi_j) \quad (76)$$

Expressions for the principal g-values were found from the resonance condition, Equation 77.

$$\Delta E = g\beta H \quad (77)$$

When the magnetic field was along the z axis, the matrix elements were calculated from:

$$H_{ij} = (\psi_i | \beta H_z(L_z+2S_z) | \psi_j) \quad (78)$$

The resonance condition then gave  $g_{zz}$ -value as expressed in Equation 79.

$$g_{zz} = 2 - \frac{2\lambda}{E(t_{2g\alpha}^a) - E(t_{2g\alpha}^c)} - \frac{6\lambda}{E(t_{2g\alpha}^a) - E(t_{2g\alpha}^c)} - \frac{\lambda^2}{2(E(t_{2g\beta}^b) - E(t_{2g\alpha}^c))(E(e_g^b) - E(t_{2g\alpha}^c))} + \frac{\lambda^2}{4(E(t_{2g\alpha}^a) - E(t_{2g\alpha}^c))^2} + \frac{\lambda^2}{4(E(t_{2g\beta}^b) - E(t_{2g\alpha}^c))^2} \quad (79)$$

$$-\frac{\lambda^2}{4(E(e_g^b) - E(t_{2g}^c))^2} - \frac{3\lambda^2}{8(E(e_g^a) - E(t_{2g}^c))^2}$$

Similar expressions were obtained for  $g_{xx}$  and  $g_{yy}$ .

## EXPERIMENTAL

## Introduction

EPR spectrometer

EPR (electron paramagnetic resonance) measurements were made on a Strand 602B, X-band, spectrometer with modifications<sup>1</sup> to the preamplifier and the modulation amplifier to facilitate the detection of broad EPR signals. The distinguishing features of the 602B spectrometer were the ferrite circulator, the adjustable reference path, the balanced mixer with a pair of crystal detectors, and the AFC (automatic frequency control). A Varian V-4531 multipurpose TE<sub>102</sub> cavity was used for all EPR measurements. A Magnion 12 inch electromagnet model L-128A provided precise magnetic fields. An NMR system utilizing a hydrogen proton probe was used to calibrate the magnetic field.

Dewars and sample arrangements

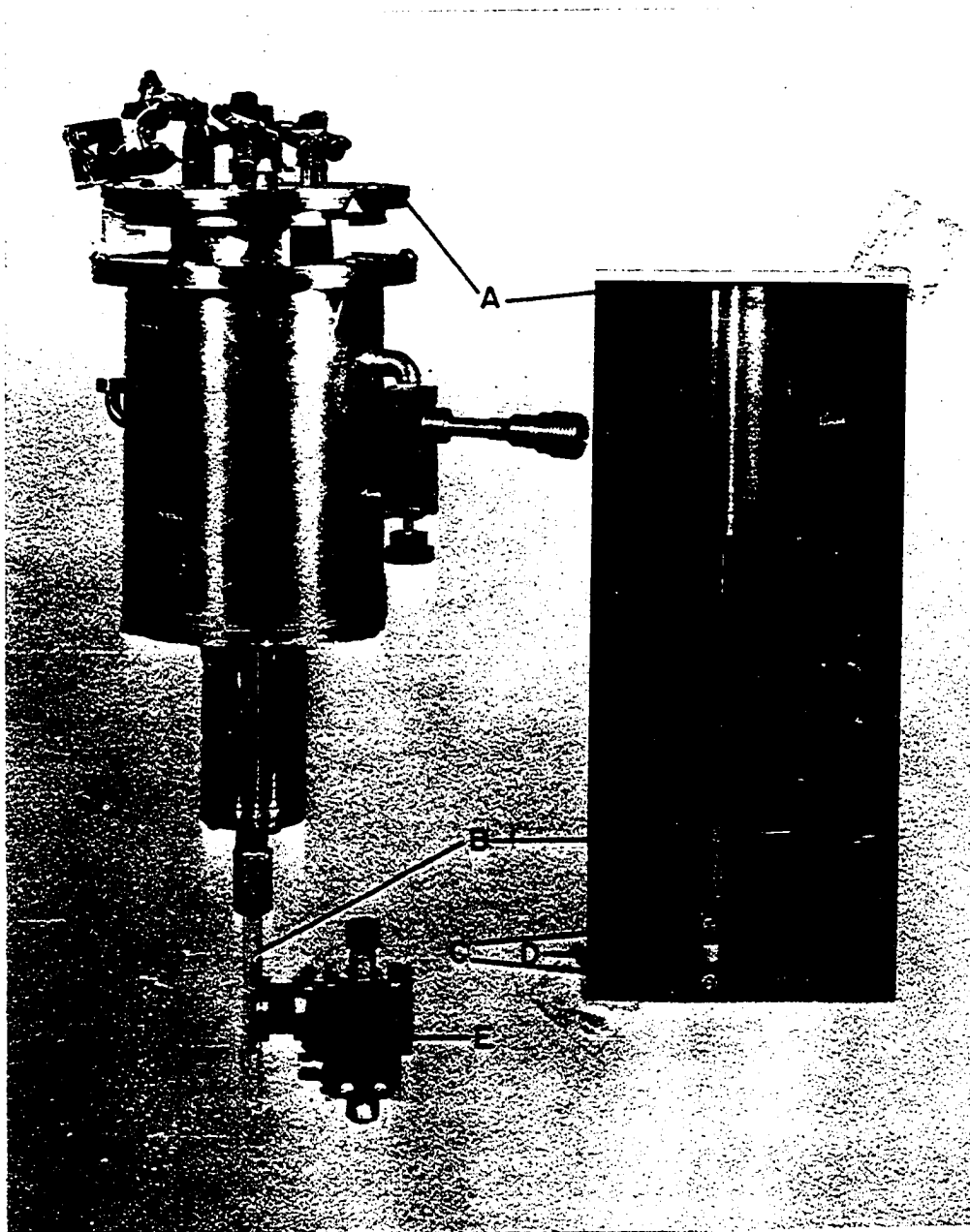
Two types of cold-finger dewars were used for all the low temperature EPR measurements. A metal cryostat<sup>1</sup> with a quartz vacuum jacket surrounding a Lucalux rod cold-finger (Fig. 3) was used for single crystal measurements. The Lucalux rod,

---

<sup>1</sup>Dr. G. A. Pearson, who was the author's supervisor between 1965 and 1969, was mainly responsible for the design of this equipment.

Fig. 3. Cryostat for rotating single crystals and for maintaining single crystals at  $77^{\circ}\text{K}$  and/or approx.  $15^{\circ}\text{K}$

- A. top of rotating helium can
- B. Lucalux rod
- C. Lucalux discs
- D. Lucalux tube
- E. Varian EPR cavity



manufactured by the Lamp and Glass Department of the General Electric Company, was attached to an inner stainless steel can. The can rested on nylon bearings so that a crystal mounted on the end of the rod could be rotated in a plane with liquid nitrogen and liquid helium in the can.

Sample buckets with screw tops were machined from boron nitride rods purchased from the Carborundum Company, Technical Ceramics Plant. Before any air-sensitive crystals were brought out of the dry box, the crystals were aligned and sealed in the bucket. The bucket was cemented onto the Lucalux rod with Apiezon N grease. The baseline spectra for the container showed EPR signals due to this sample container. Two low field resonances due to Lucalux were observed below 2000 gauss and in no way interfered with the metal complex spectra. In addition, a sharp peak and a broad peak were observed for the BN bucket. The sharp peak served as a convenient reference peak, the broad peak between 2000 and 5000 gauss was superimposed on the metal complex spectra.

A sample container was also made from a Lucalux rod with two Lucalux plates (Fig. 3) cemented over the open ends of the rod with Apiezon W. The baseline from this container was resonance free except for the Lucalux peaks mentioned in the

preceding paragraph.

Powder and glass samples were sealed in quartz tubes and placed in a quartz cold-finger (Fig. 4). The dewar was filled with liquid nitrogen and the finger inserted into the Varian cavity. To prevent bubbling in the cavity, helium gas was forced through a heat exchanger and allowed to escape above the sample.

#### Visible and infrared equipment

Reflectance spectra of powdered  $\text{NbBr}_4\text{Ac}_2$  were measured on a Beckman DU spectrophotometer equipped with the Beckman 2580 reflectance attachment. The  $\text{NbBr}_4\text{Ac}_2$  powder was diluted with dry  $\text{MgCO}_3$ ; dry  $\text{MgCO}_3$  was used for the reference.

The absorption spectra of acetonitrile solutions in the visible and near-infrared were measured on a Cary 14 spectrophotometer using Pyrocell S22-350 rectangular fused silica cells.

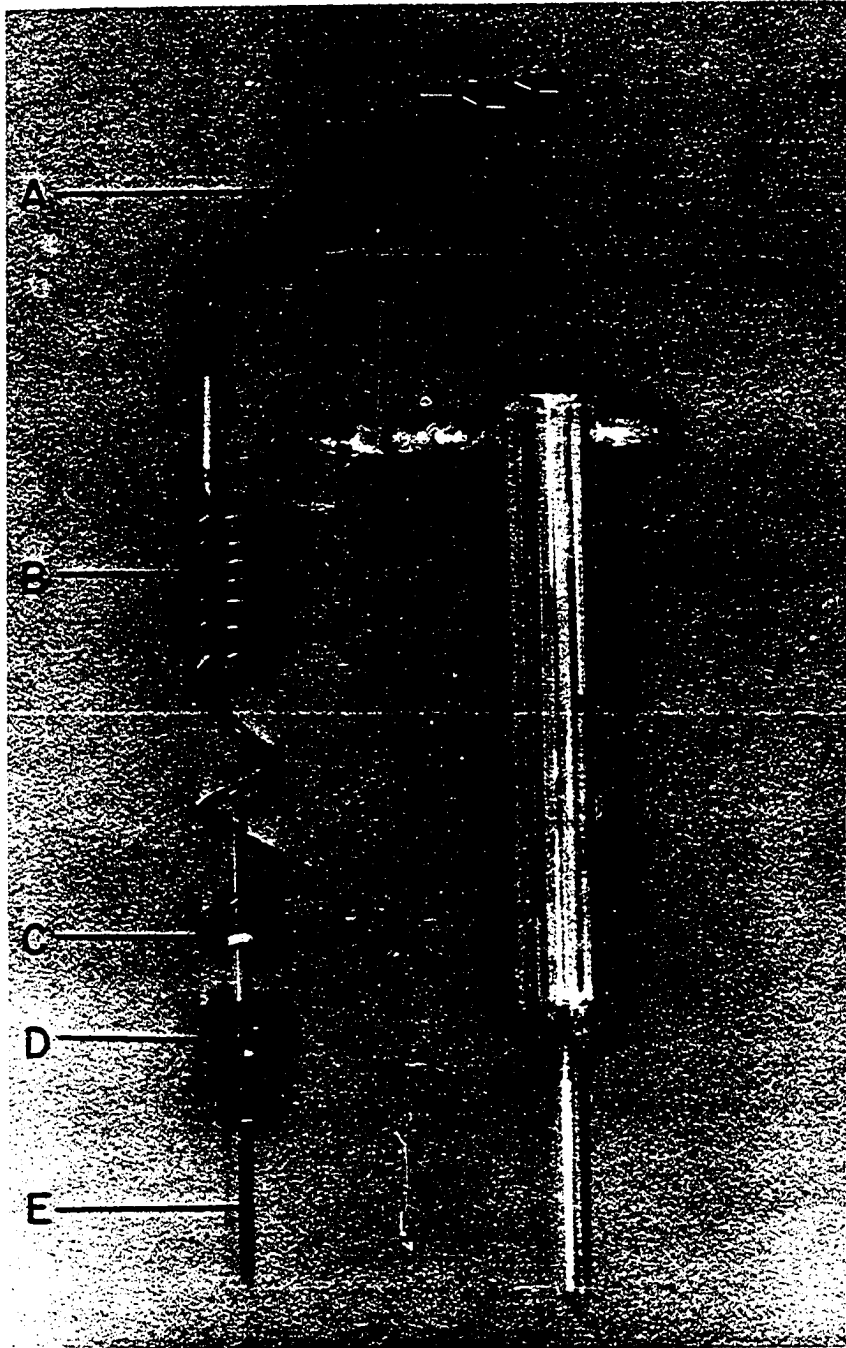
#### Crystals

Crystals of  $\text{NbBr}_4\text{Ac}_2$  were grown in vacuo in the apparatus pictured in Fig. 5. In an argon filled dry box, powder was placed in side A, the apparatus was removed from the dry box and coupled to a vacuum line, and acetonitrile was distilled into side A. The apparatus was heated in a water bath to



Fig. 4. Quartz dewar (right) and sample arrangement (left)  
for maintaining powder and glasses at 77°K

- A. tubing connected to helium gas cylinder
- B. coiled copper tubing
- C. holes (approx. .4 mm diameter) on bottom of coil
- D. sample holder
- E. 2 mm O.D. quartz sample tube



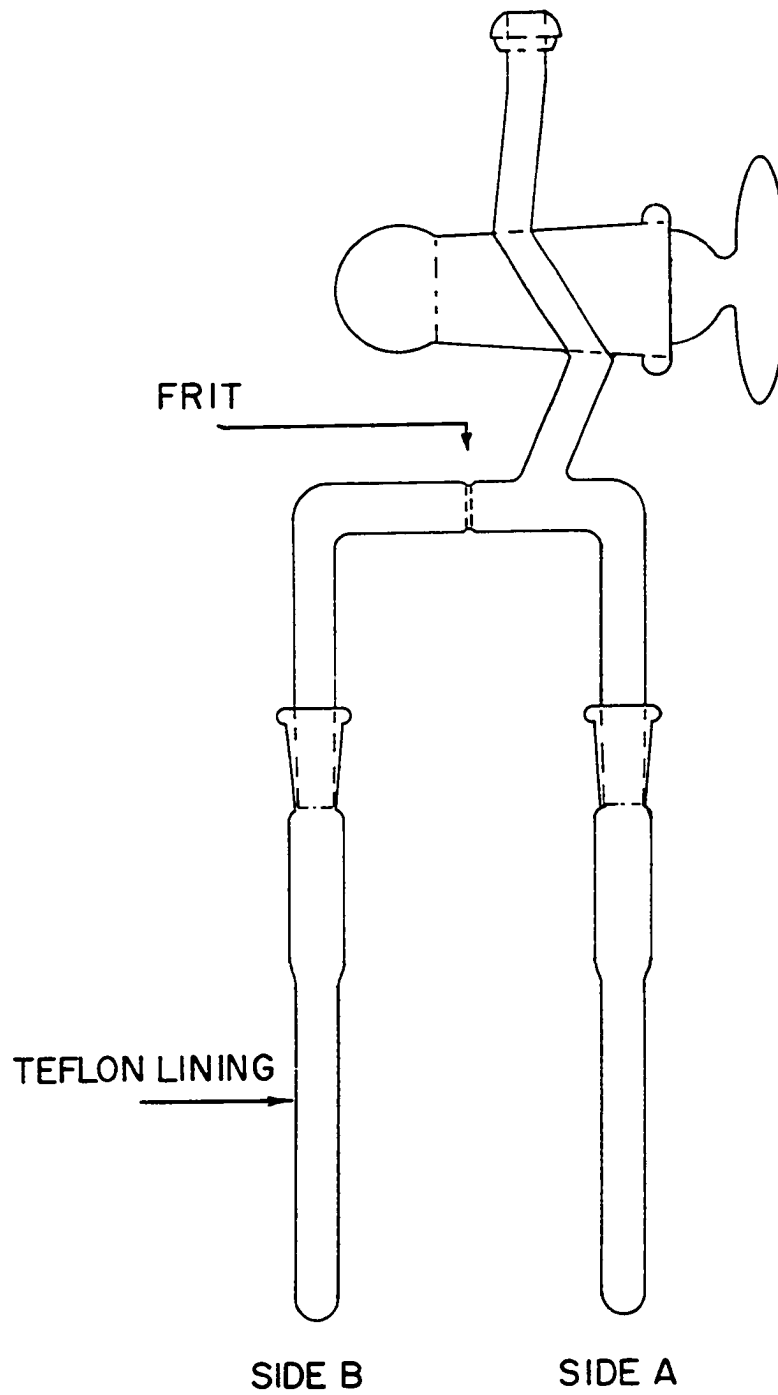


Fig. 5. Crystal growing apparatus

approximately  $60^{\circ}\text{C}$  before the saturated solution was transferred to side B. The apparatus was placed in a styrofoam-capped dewar filled with water at  $60^{\circ}$  and allowed to stand for two days. At this time, the solvent was pumped off and, after the sample was pumped into the dry box, the crystals were removed from the Teflon and stored in the dry box.

### EPR of $\text{NbBr}_4\text{Ac}_2$

#### Powder

Spectra at room temperature were not observed for the  $\text{NbBr}_4\text{Ac}_2$  powder. The EPR spectrum of  $\text{NbBr}_4\text{Ac}_2$  powder at liquid nitrogen ( $77^{\circ}\text{K}$ ) temperature was reproduced in Fig. 6. The peak to peak spread was approximately  $1000 \pm 100$  gauss and  $g = 1.65 \pm .03$ . No obvious anisotropy or hyperfine structure was apparent.

#### Crystals

The crystallographic axes of  $\text{NbBr}_4\text{Ac}_2$  crystals were determined by X-ray techniques using oscillation and zero-level Weissenberg photographs. Crystals of  $\text{NbBr}_4\text{Ac}_2$  have well formed rectangular faces and are usually thin plates. Crystals were aligned in a sample container in an argon filled dry box using a microscope and held securely in place with Apiezon N or halocarbon grease. Since the crystals, along with the

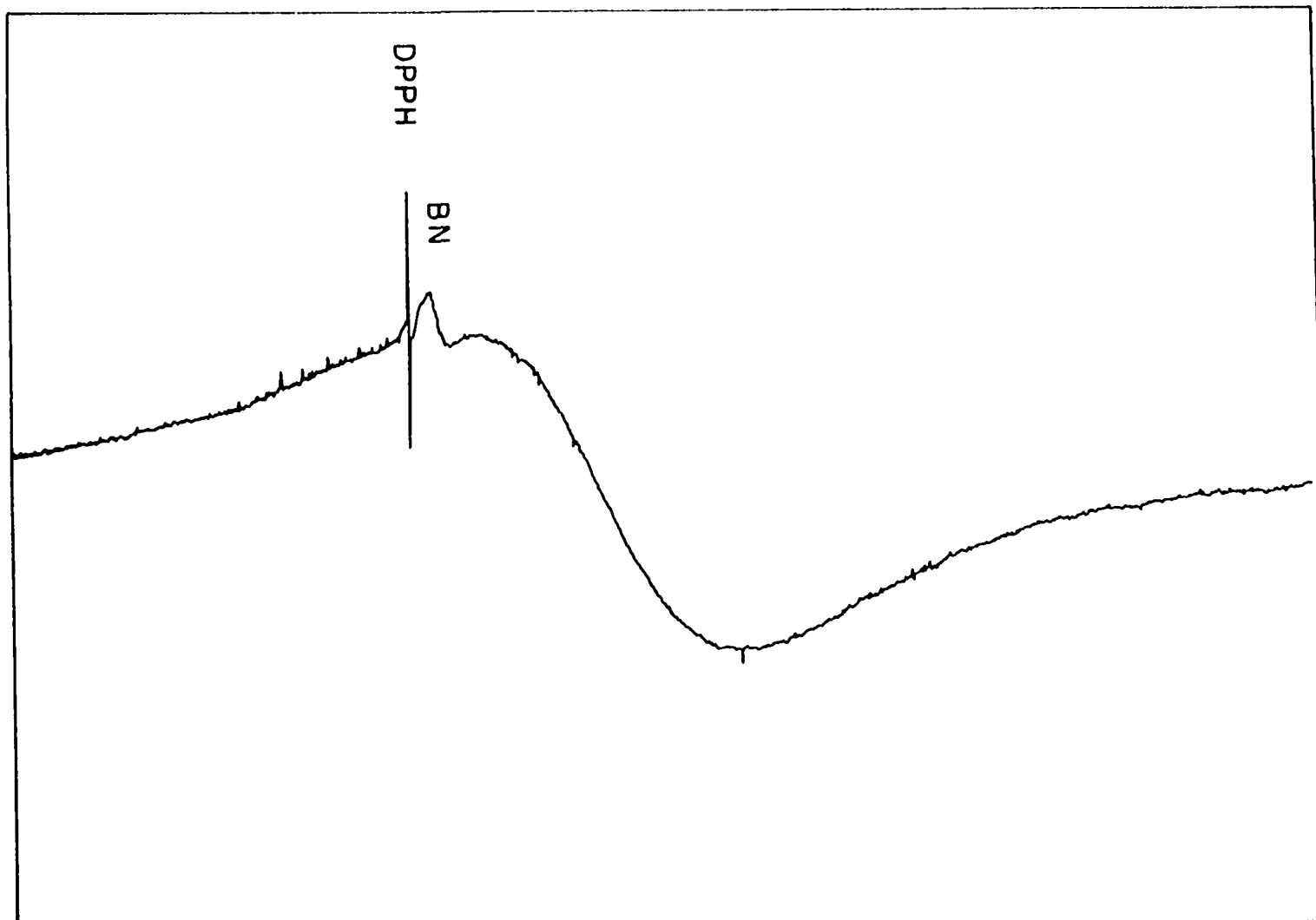


Fig. 6. EPR powder spectrum of  $\text{NbBr}_4(\text{CH}_3\text{CN})_2$  at  $77^\circ\text{K}$  (the magnetic field is increasing from left to right)

quality of the spectra, sometimes deteriorated with time, the best spectra were obtained immediately after the sample was cooled in the cryostat. Also, for each single crystal in which zero-level Weissenberg and oscillation photographs had been taken, EPR spectra as a function of rotation angle were observed for no more than two of the three crystal planes before the crystal deteriorated.

Again room temperature spectra were not observed for  $\text{NbBr}_4\text{Ac}_2$  single crystals. The spectrum of a crystal of undetermined orientation was compared at liquid nitrogen and liquid helium temperatures. Because the g-value and peak to peak separation were not altered, subsequent measurements were made only with liquid nitrogen coolant.

EPR spectra as a function of rotation angle were recorded for the three crystallographic planes and g-values were plotted against the angle a crystallographic axis makes with the magnetic field. Typical spectra for the b-c plane are presented in Fig. 7 and g-value maps have been plotted in Figs. 8, 9, and 10.

The error in the experimental g-values depended upon the accuracy with which the maximum for the absorption peaks could be determined. The  $\text{NbBr}_4\text{Ac}_2$  single crystal EPR spectra were

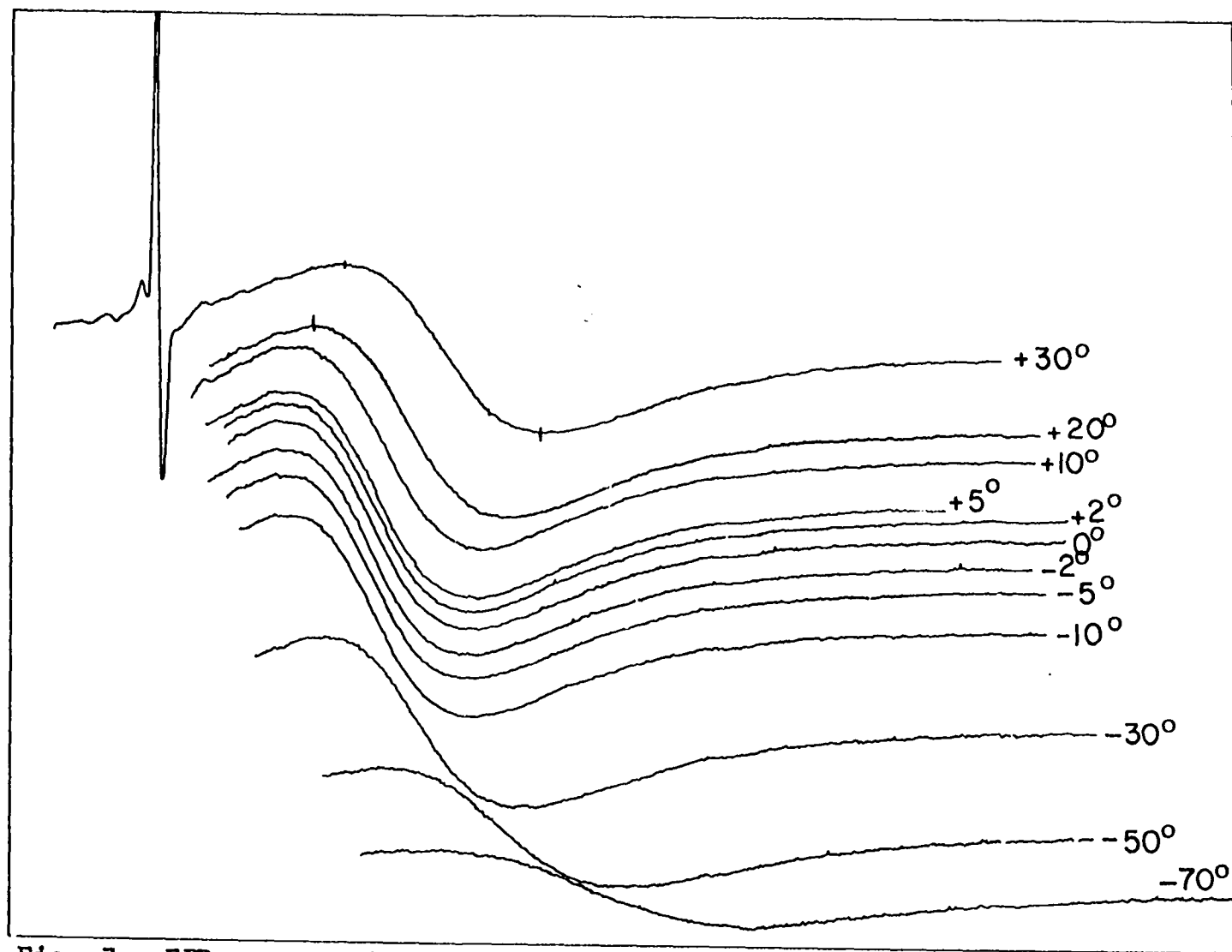


Fig. 7. EPR spectra in  $b$ - $c$  crystal plane of  $\text{NbBr}_4(\text{CH}_3\text{CN})_2$  at  $77^\circ\text{K}$  as a function of the angle between the magnetic field and the  $b$ -crystal axis (the magnetic field is increasing from left to right)

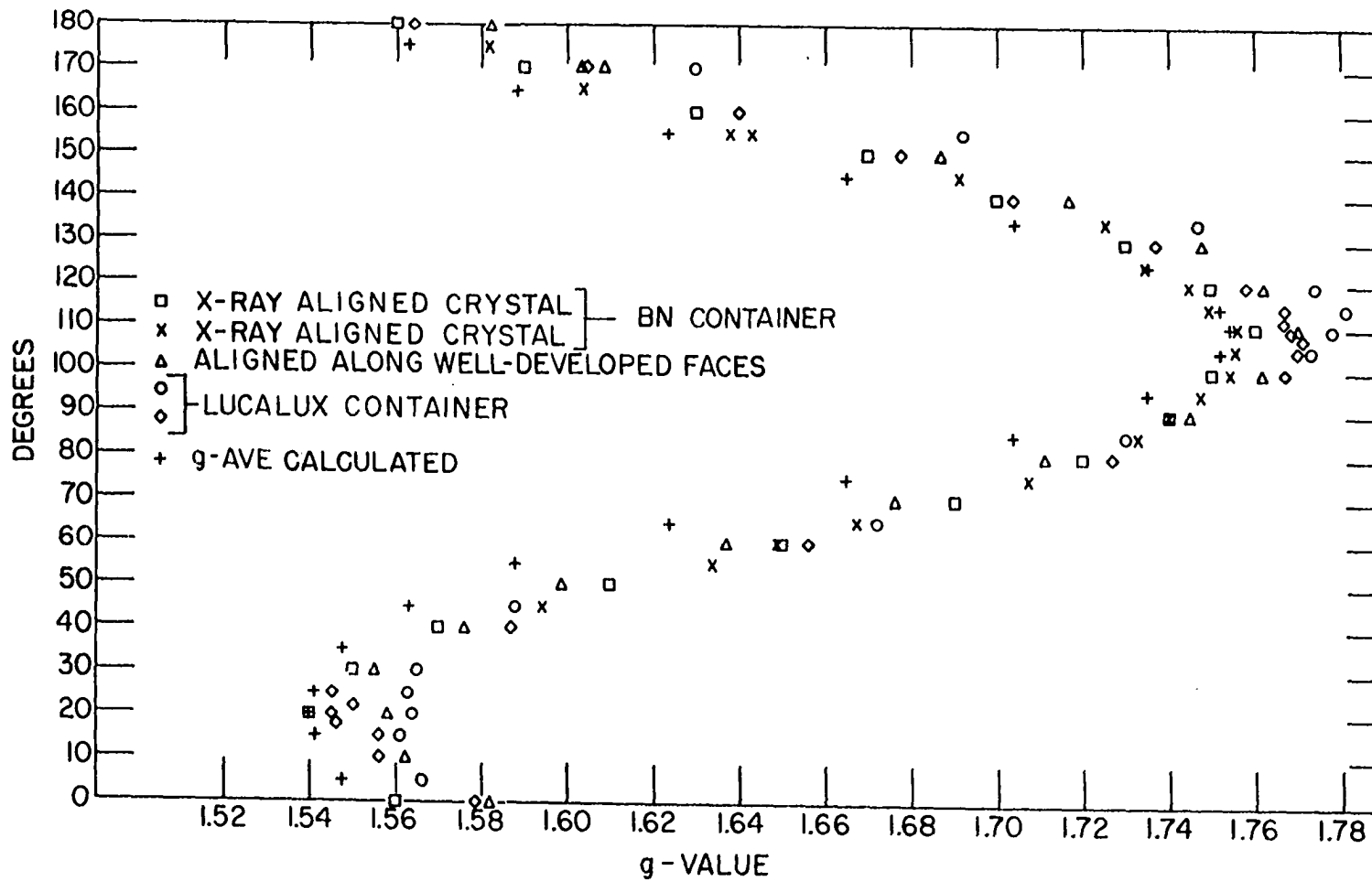


Fig. 8. EPR single crystal data for  $\text{NbBr}_4(\text{CH}_3\text{CN})_2$  in the b-c plane



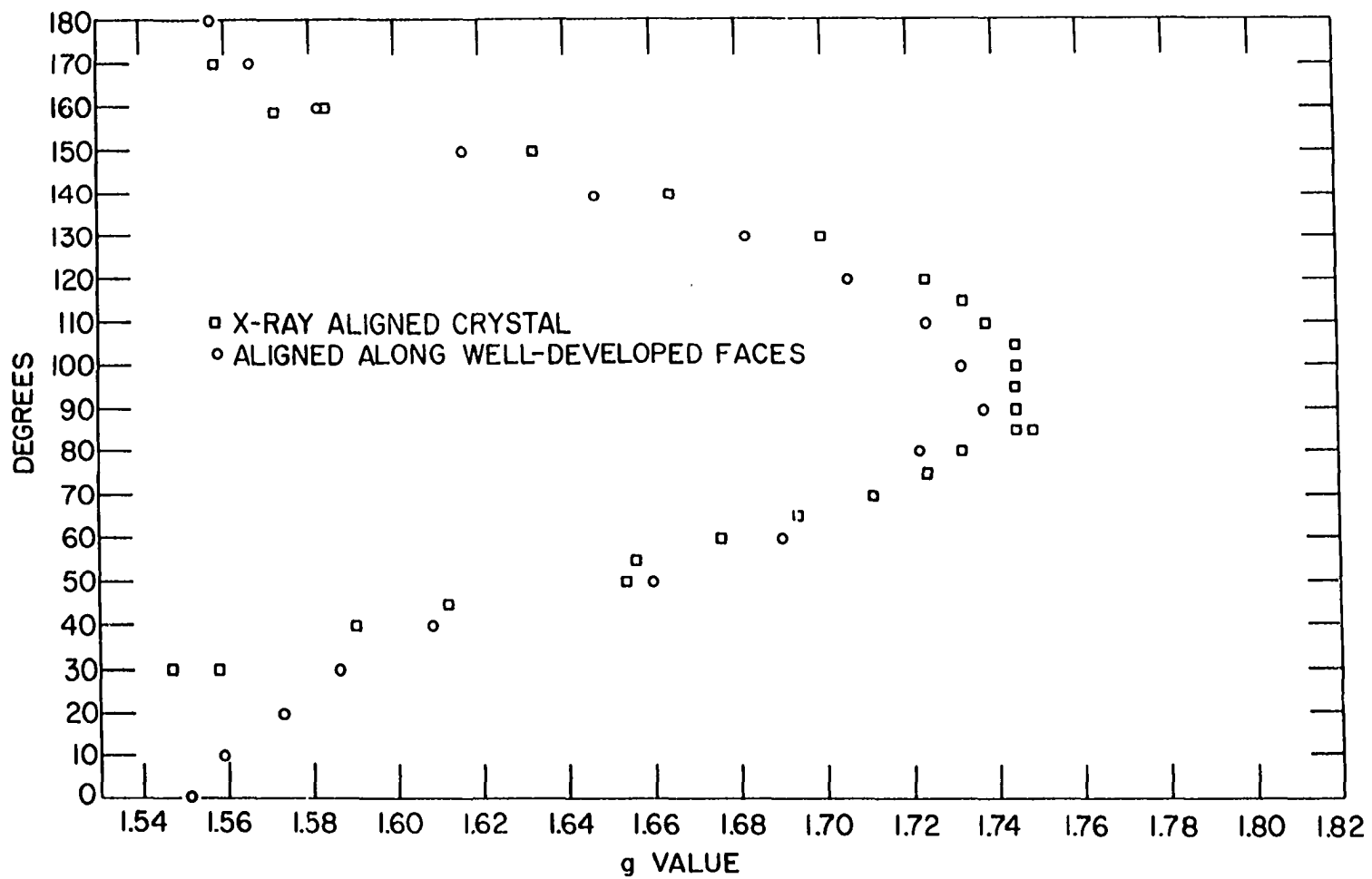


Fig. 9. EPR single crystal data for  $\text{NbBr}_4(\text{CH}_3\text{CN})_2$  in the a-c plane

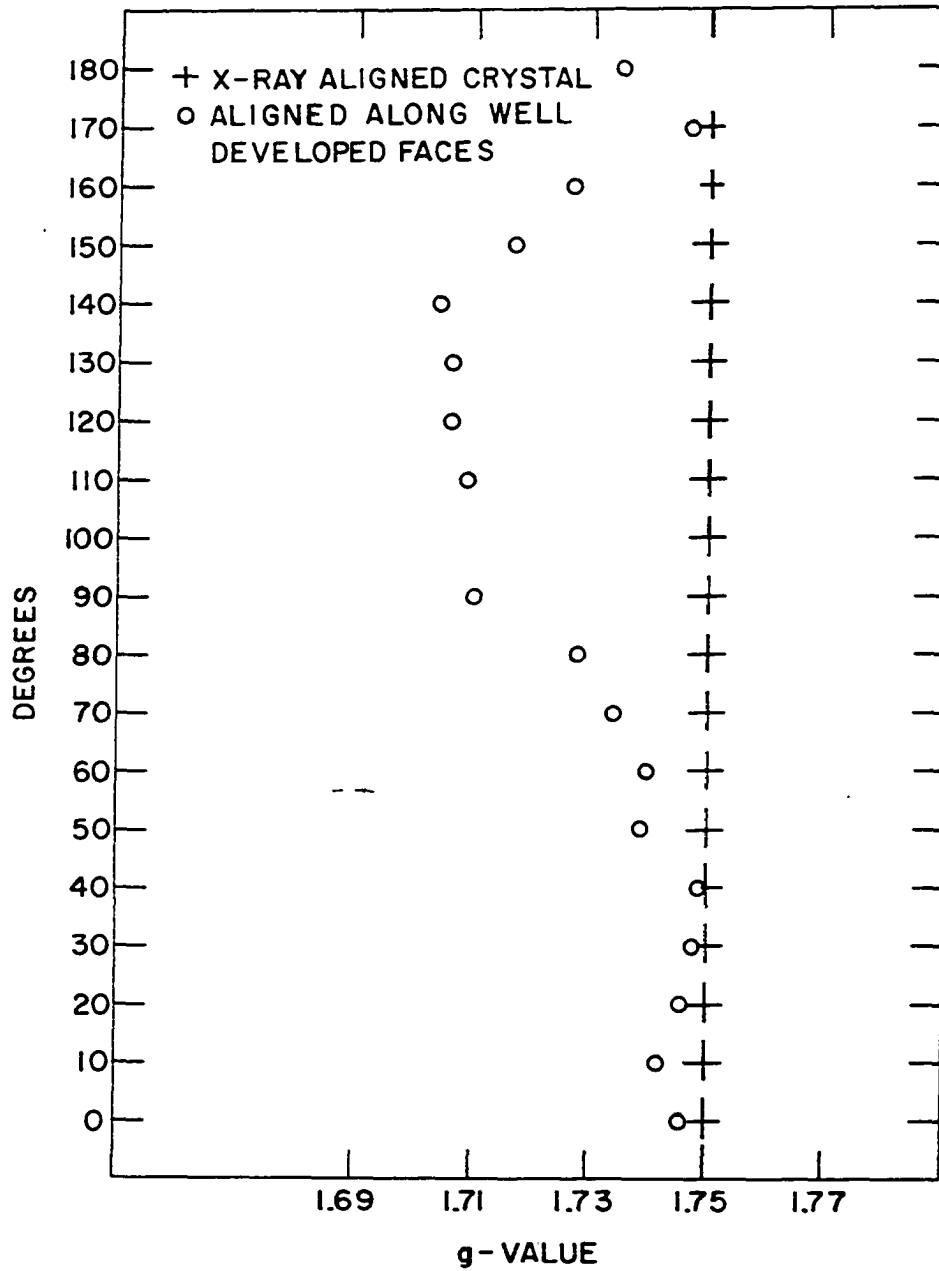


Fig. 10. EPR single crystal data for  $\text{NbBr}_4(\text{CH}_3\text{CN})_2$  in the a-b plane

recorded as the derivative of the absorption peak where the maximum absorption was the midpoint of the S-shaped derivative curve or the point in the center of the S-shaped curve with the same ordinate as the resonance free baseline. For symmetrical spectra the g-value was also taken as the point midway between the peak to peak separation. For most of the spectra in Fig. 7 the g-values agreed within 0.01 g-value units regardless of the method used to determine the absorption maximum. The measurements were more precise than accurate, i.e. the g-values for the experimental data from the same crystal mapped in Fig. 7 were consistently larger or smaller than the average for the experimental g-values.

From the crystal structure of  $\text{NbBr}_4(\text{Ac})_2$  (2), the g-tensor was diagonalized and the direction and magnitude of the principal g-values were found. The four molecules in the unit cell were related by a screw axis and two glide planes and complicated the determination of the principal g-values. When the magnetic field was along the crystal axes, the molecules in the unit cell were magnetically equivalent. When the magnetic field was not along the crystal axes, all the molecules in the unit cell were not magnetically equivalent. Additional EPR spectra were expected for each magnetically

inequivalent site.

When the magnetic field was along the a crystal axis, the magnetic field was also along the axis of quantization, i.e. the z axis in Fig. 1, for all four molecules in the unit cell. The g-value extracted with the magnetic field along the z direction was  $g_{zz}$  equal to  $1.75 \pm 0.04$ . The deviation in Fig. 10 for the crystal aligned along well developed faces, where the crystal axes were not determined from X-ray photographs, was probably due to imperfect alignment.

For the x-y plane the principal axes were not aligned along the crystal b-c axes. The b and c crystal axes were the three-fold axes in octahedral symmetry except, instead of the equivalent ligands for octahedral symmetry, two bromine atoms and an acetonitrile ligand were situated above and below the niobium atom. Therefore, along the b and c crystal axes the four molecules per unit cell were also magnetically equivalent and contributed to a single EPR resonance.

For other directions in the x-y plane the four molecules per unit cell had two magnetically inequivalent sites. That is, each pair of magnetically equivalent molecules in the unit cell were related to each other by a two-fold rotation

along the x-axis of Fig. 1. One then expected to see two resonances - one for each inequivalent site - as the molecule was rotated in the x-y plane. However, only one resonance per given direction was observed for rotation in the x-y and/or b-c plane as shown in Fig. 7. If the behavior of the Nb complex was analogous to, for instance, some copper(II) complexes (31), the single resonance could easily be explained due to exchange interactions. In order to separate exchange coupled resonances, one would require a variable temperature cryostat and several higher microwave frequencies which were not available for the present EPR spectrometer.

The assumption was made that the g-value observed was an average of two g-values from inequivalent sites. First  $g_1$  and  $g_3$  were calculated from the equivalent positions along the axes. Then,  $g_1$  and  $g_3$  were substituted into an equation for the average g-value. Calculated g-values for directions off the crystal axes were compared with the experimental g-values.

Considering the x-molecular axis in Fig. 1 as the reference axis:

$$g_{ave} = \frac{1}{2}[(g^2)_{xx} \cos^2\theta + (g^2)_{yy} \sin^2\theta]^{\frac{1}{2}} \quad (80)$$

$$+ \frac{1}{2}[(g^2)_{xx} \cos^2\theta + (g^2)_{yy} \sin^2\theta]^{\frac{1}{2}}$$

where  $\cos\theta$ ,  $\sin\theta$ ,  $\cos\phi$ , and  $\sin\phi$  formed the direction cosines relative to the molecular axis and  $(g^2)_{xx}$  and  $(g^2)_{yy}$  were the principal values of the  $g^2$ -tensor.

For the magnetic field along the  $\underline{c}$  axis, the x axis of one site formed an angle of -55 degrees with the magnetic field and the x-axis of the other site formed an angle of +55 degrees with the magnetic field.

$$g_c = [(g^2)_{xx} \cos^2 55 + (g^2)_{yy} \sin^2 55]^{\frac{1}{2}} = 1.55 \pm .03 \quad (81)$$

For the magnetic field along the  $\underline{b}$  axis, the x axis of one site formed an angle of +35 degrees with the magnetic field and the x-axis of the other site formed an angle of 145 degrees with the magnetic field.

$$g_b = [(g^2)_{xx} \cos^2 35 + (g^2)_{yy} \sin^2 35]^{\frac{1}{2}} = 1.77 \pm .02 \quad (82)$$

Solving these equations for  $g_{xx}$  and  $g_{yy}$  gave:

$$g_1 = g_{xx} = 1.95 \pm .06 \quad (83)$$

$$g_3 = g_{yy} = 1.30 \pm .06 \quad (84)$$

$$g_2 = g_{zz} = 1.75 \pm .04 \quad (85)$$

Then,  $g_1$  and  $g_3$  were substituted in the equation for  $g_{ave}$  and the map for calculated  $g_{ave}$  assumed the same angular dependence as the map for experimental  $g_{ave}$  (Fig. 7).

## Glasses

In order to resolve the g-value and hyperfine components from the spectra of  $\text{NbBr}_4\text{Ac}_2$ , the niobium(IV) complex was dissolved in solvents which were expected to form suitable glasses. The logical choice was acetonitrile, but a poor glass and unresolved spectra were obtained. After considerable searching, a 75:25 mixture of toluene to acetonitrile was found to form a clear glass and to hold enough  $\text{NbBr}_4\text{Ac}_2$  in solution (.05M) for an intense X-band spectrum to be recorded.

The  $\text{NbBr}_4\text{Ac}_2$  glass spectrum shown in Fig. 11 contained ten hyperfine lines for which  $g_{xx}$  was equal to  $1.91 \pm 0.03$  and the coupling constant for the separation between the second and third peak was  $268 \pm 20$  gauss. In addition to the broad resonance on the high field side, unresolved EPR resonances due to the  $g_{zz}$  and  $g_{yy}$  components were observed under the hyperfine lines for the  $g_{xx}$  component. Niobium has a nuclear spin of  $9/2$  and lack of resolution may be due to the large number of overlapping  $\Delta m_I = 0$  and  $\Delta m_I > 0$  transitions, i.e. quadrupole effects (32). Unfortunately the baseline was not resonant free and was not reproducible from sample to sample. Therefore, no attempt was made to fit the spectrum

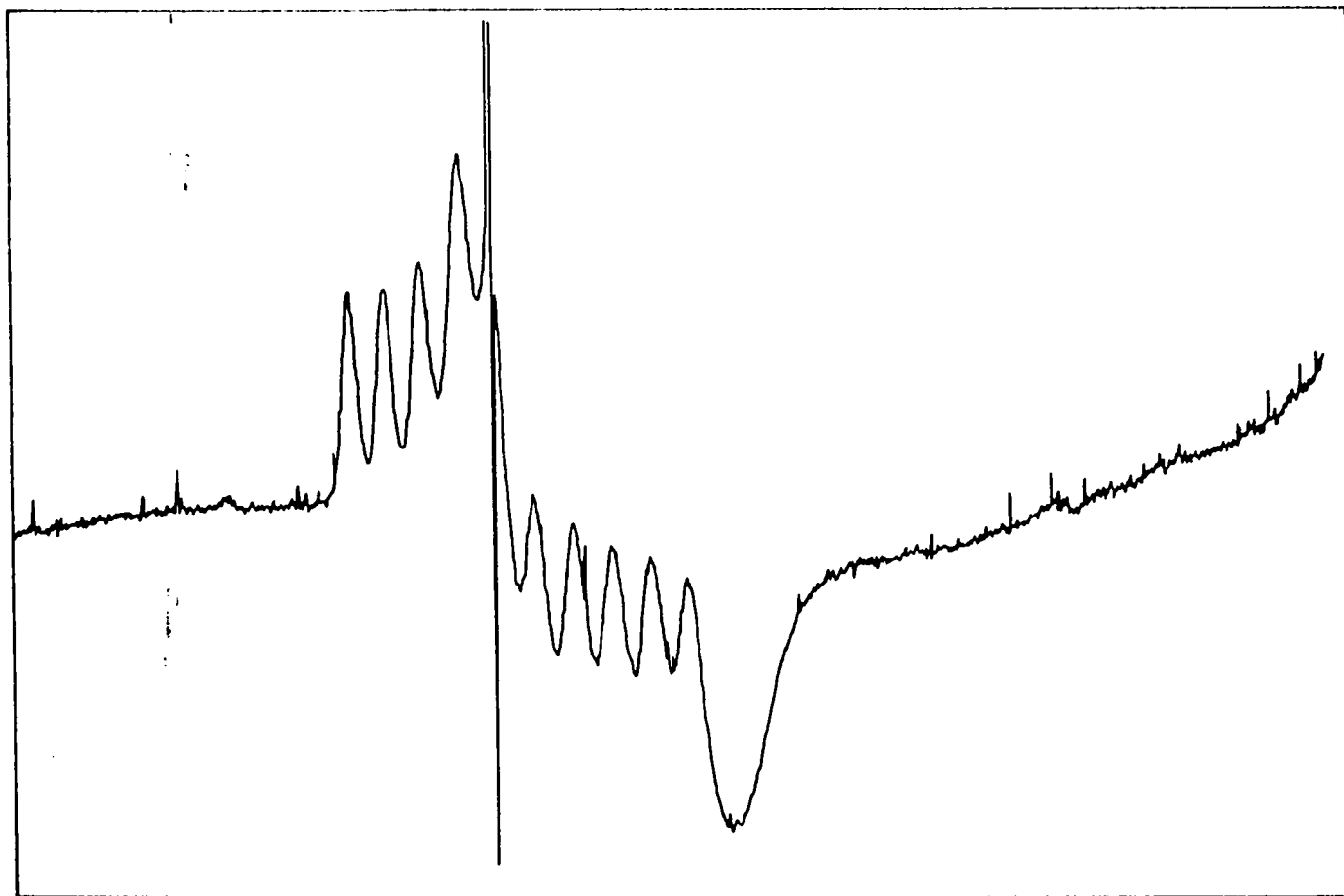


Fig. 11. EPR spectrum of  $\text{NbBr}_4(\text{CH}_3\text{CN})_2$  trapped in an acetonitrile-toluene glass at  $77^\circ\text{K}$  (the magnetic field is increasing from left to right)



in detail, but a computer program<sup>1</sup> was used to simulate the glass spectrum given the intensity, x-scale factor in gauss/cm, the line width, and nuclear spin of the particle.

The simulated spectrum was just the sum of the proposed hyperfine lines for the three different g-values. In Fig. 12 the upper curve was the proposed spectrum formed from the resolved experimental hyperfine lines around  $g_{xx}$ . For the lower curve in Fig. 12, a ten line spectrum with a line shape similar to the upper curve in Fig. 12 was proposed except the half-width of the hyperfine lines was increased to 350 gauss such that the hyperfine components (approximately 250 gauss coupling constant) were no longer resolved. The spectrum was reflected along the abscissa as expected for the  $g_{yy}$  component. In Fig. 13 a ten line spectrum was simulated where the half-width was small compared to the coupling constant. For the lower curve in Fig. 13, the half-width was increased to 350 gauss and the coupling constant was 150 gauss. Arbitrarily fitting the hyperfine components together in order to obtain the experimental line shape gave the simulated spectrum with  $g_1$  equal to 1.91,  $g_2$  equal to 1.65, and  $g_3$  equal to 1.54 - a

---

<sup>1</sup>This program, which assumed a Lorentzian line shape for the parent line, was borrowed from Dr. T. Couch, Ames Laboratory, Iowa State University.

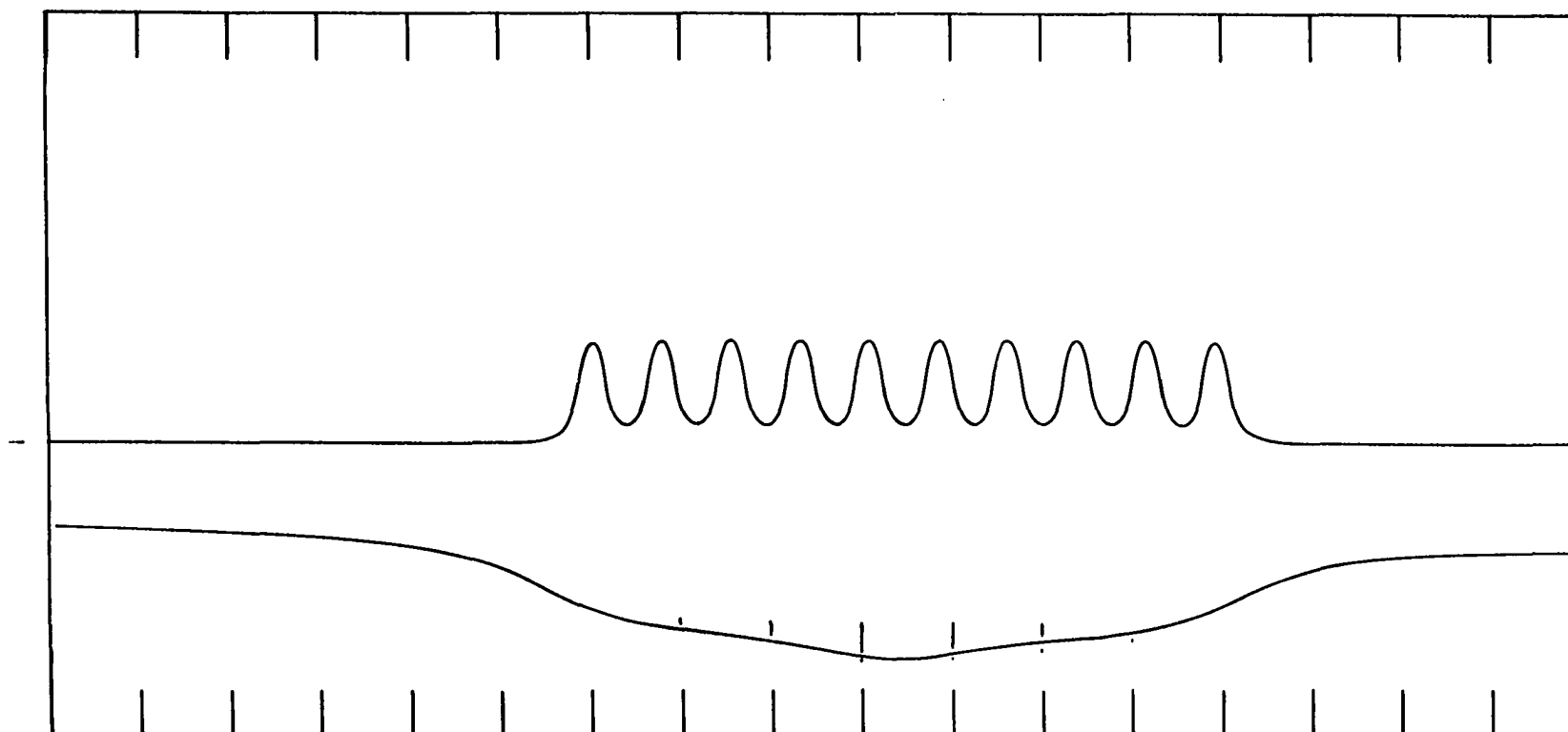


Fig. 12. Simulated spectra for  $g_1$ -value with hyperfine line width of 175 gauss (upper curve) and for  $g_3$ -value with increased hyperfine line width of 350 gauss (lower curve)

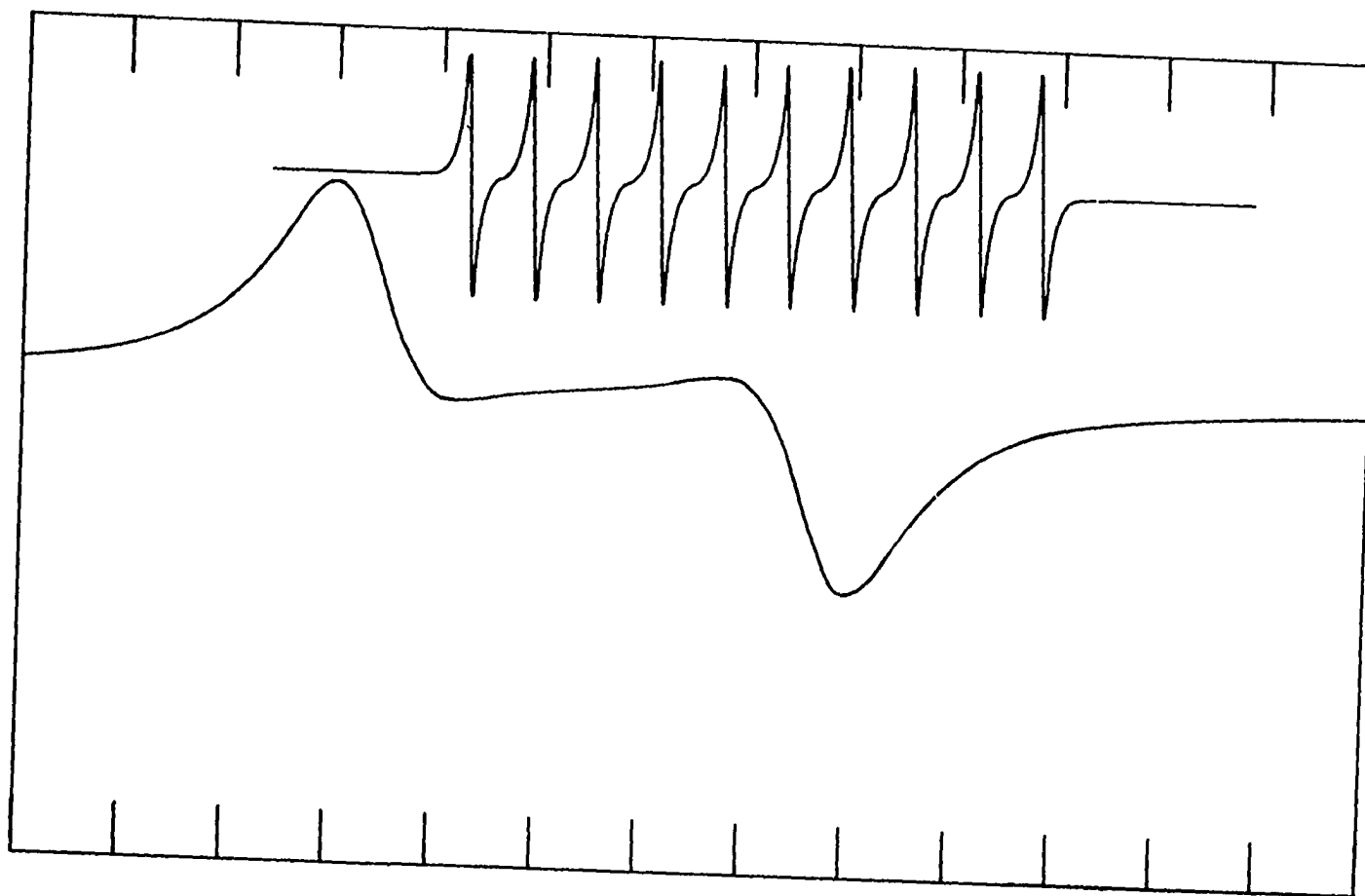


Fig. 13. Simulated spectra for  $g_2$ -value with hyperfine line width of 15 gauss (upper curve) and increased line width of 350 gauss (lower curve)

rough fit (Fig. 14).

If the baseline accounted for a portion of the drop in the line shape following the DPPH signal, then the hyperfine coupling constant for the  $g_{yy}$  component may be much less than 250 gauss and the  $g_3$  component may be confined under the unresolved high field peak. Then  $g_{zz}$  and  $g_{yy}$  values nearly conformed to  $g_{zz}$  equal to 1.75 and  $g_{yy}$  equal to 1.30 from the crystal work.

#### Future work

While investigating the magnetic properties of the  $\text{NbBr}_4\text{Ac}_2$  system, other directions that led to inconclusive results were described here in the hope that this research may prove beneficial for future work on low-symmetry  $d^1$  transition metal complexes.

An attempt was made to obtain EPR data from  $\text{NbBr}_4\text{Ac}_2$  diluted in a diamagnetic host,  $\text{ZrBr}_4\text{Ac}_2$ . From the powder patterns, different space groups were assigned to the  $\text{NbBr}_4\text{Ac}_2$  and  $\text{ZrBr}_4\text{Ac}_2$  complexes. Crystals with approximately 25 percent  $\text{NbBr}_4\text{Ac}_2$  and 75 percent  $\text{ZrBr}_4\text{Ac}_2$  were grown out of acetonitrile solution and had the  $\text{ZrBr}_4\text{Ac}_2$  powder pattern. The EPR spectrum at liquid nitrogen temperatures for an unoriented crystal of this type had the ten hyperfine lines characteris-

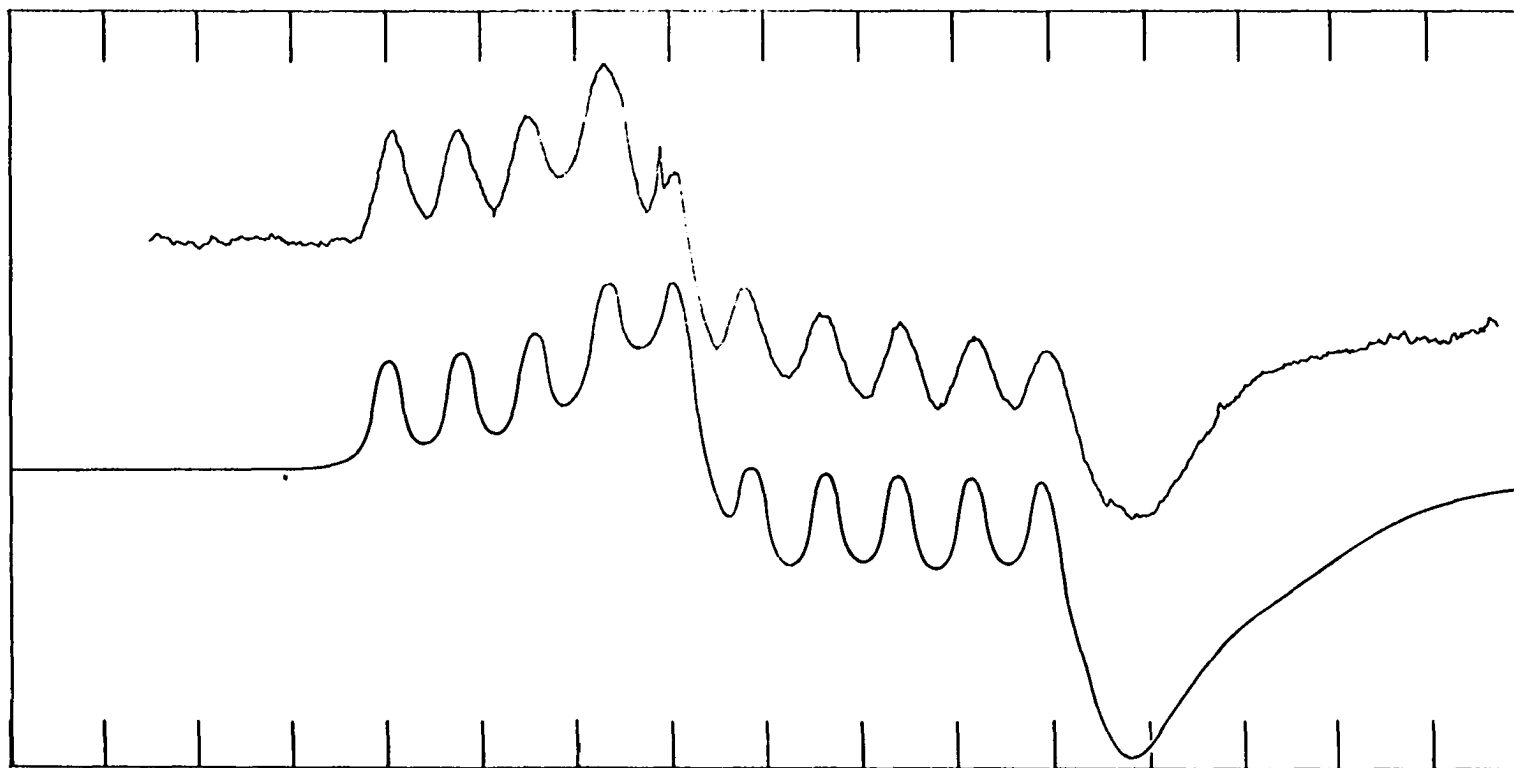


Fig. 14. EPR spectrum of  $\text{NbBr}_4(\text{CH}_3\text{CN})_2$  in acetonitrile-toluene glass at  $77^\circ\text{K}$  (upper curve) compared with simulated EPR spectrum (lower curve)

tic of spin 9/2 for the niobium nucleus. Oscillation and zero-level Weissenberg photographs indicated disorder in one of the planes of the diluted crystals. Attempts to grow single crystals of  $ZrBr_4Ac_2$  were unsuccessful because the Zr(IV) complex, which looked crystalline in solution, cracked when the solvent was pumped away from the complex. The ordering in the crystals seemed to be proportional to the percentage of niobium(IV) complex in the mixture.

A powdered sample of  $ZrBr_4Ac_2$  containing 10 percent Nb melted at  $230^{\circ}C$ . The EPR line shape for  $NbBr_4Ac_2$  in the quenched melt (Fig. 15) coincided with the line shape for  $NbBr_4Ac_2$  in the acetonitrile-toluene glass. In fact, more structure for the high field  $g_{yy}$  component seemed resolved in the melt than in the glass.

In addition to studying the exchange interaction in  $NbBr_4Ac_2$  single crystals at Q-band and higher microwave frequencies (pg 55), Q-band (microwave frequency of approximately 35 gigacycles) spectra could also be used to separate the hyperfine lines for the anisotropic g-values of  $NbBr_4Ac_2$  in the acetonitrile-toluene glass. For example, X-band spectra for  $NbBr_4Ac_2$  had g-values at 3000, 3400, and 4600 gauss, whereas Q-band spectra should have the same g-values at

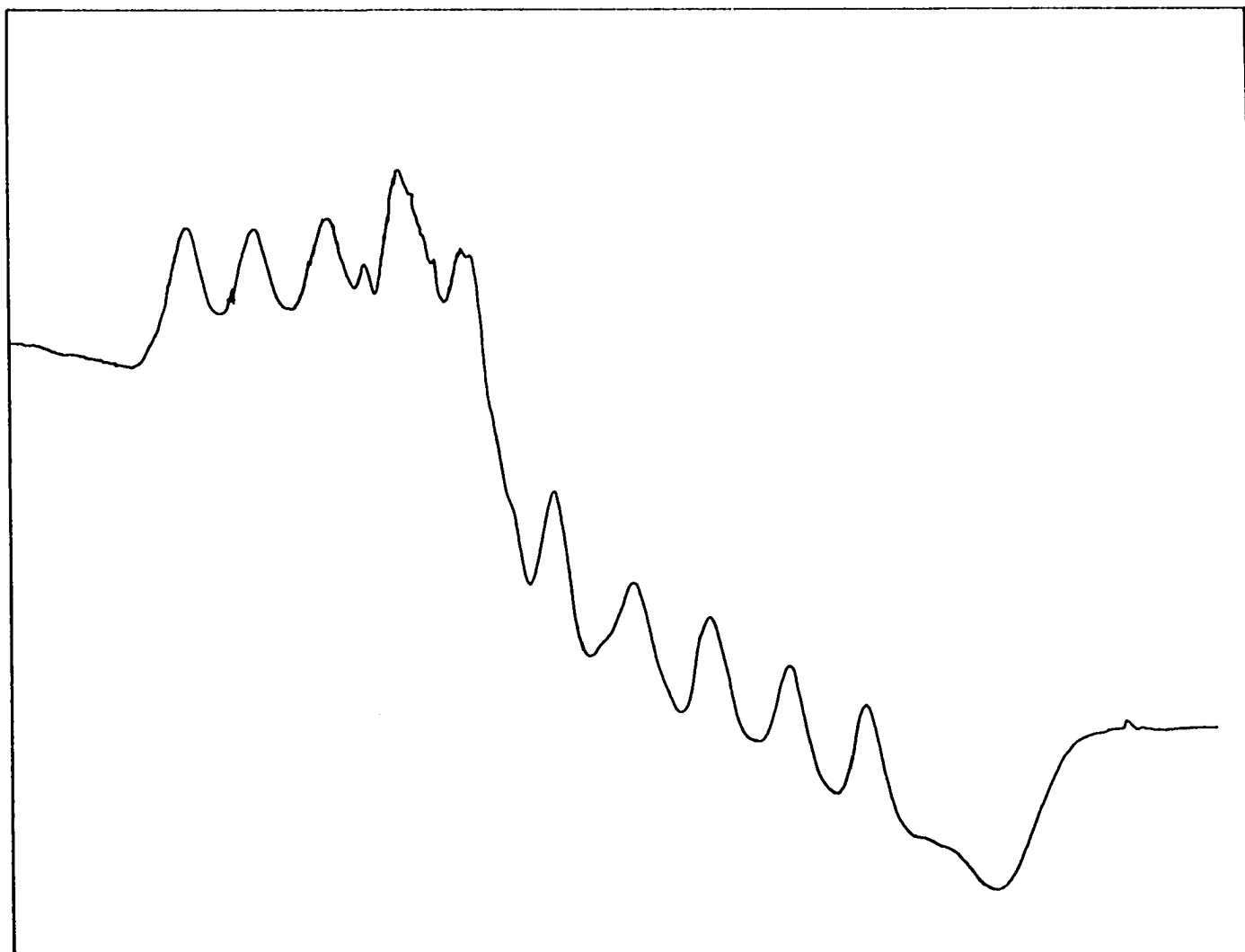


Fig. 15. EPR spectrum of quenched melt of 10%  $\text{NbBr}_4(\text{CH}_3\text{CN})_2$  and 90%  $\text{ZrBr}_4(\text{CH}_3\text{CN})_2$  at  $77^\circ\text{K}$  (the magnetic field is increasing from left to right)

approximately 12,000, 13,600, and 18,400 gauss. The coupling constant in gauss remains unchanged for X-band and Q-band so that the hyperfine lines for the  $g_{xx}$ ,  $g_{yy}$ , and  $g_{zz}$  components are separated from each other.

Solvents were mixed with  $NbBr_4$  to determine if the solvents would make suitable non-reactive glasses. Interesting, but as yet uninterpreted, spectra were found for bis(2-methoxyethyl)ether,  $CH_3OCH_2CH_2OCH_2CH_2OCH_3$  (Fig. 16) and 2-methyl THF (Fig. 17). Four or five low field peaks were resolved before the hyperfine components overlapped. Forbidden and  $\Delta m > 1$  quadrupole transitions plus low symmetry anisotropy should be considered when predicting the spectra.

#### Electronic Spectra of $NbBr_4Ac_2$

Torp (1) recorded the ultraviolet, visible, and near infrared absorption spectra for the  $NbBr_4Ac_2$  complex. From the solution spectrum of the niobium(IV) complex in acetonitrile and from the diffuse reflectance spectrum of the solid complex, three transition energies - 24,700  $cm^{-1}$  ( $\epsilon_{max}$  380), approximately 19,100  $cm^{-1}$  ( $\epsilon_{max}$  approximately 20), and less than or equal to 4000  $cm^{-1}$  ( $\epsilon_{max}$  approximately 20) - were assigned to the metal d-d transitions.

The reflectance spectrum and the solution spectrum were redetermined in this work and agreed with Torp's spectra.



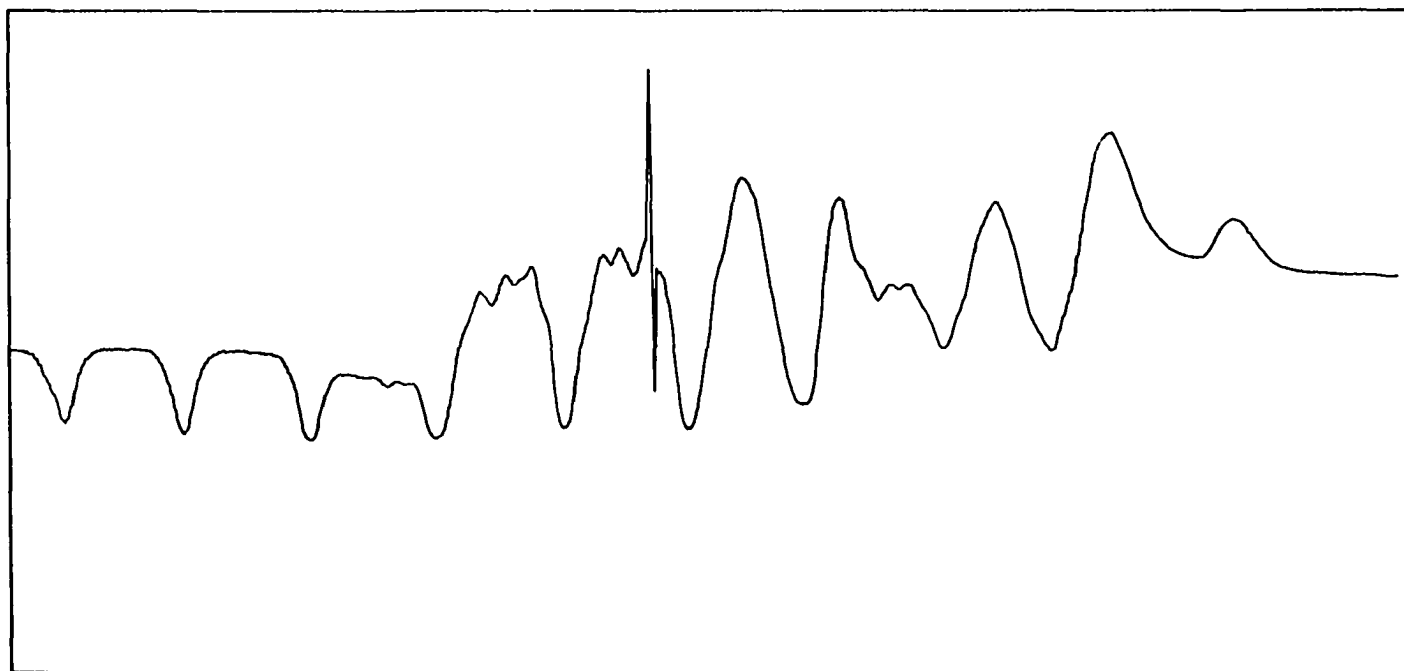


Fig. 16. EPR spectrum of  $\text{NbBr}_4$  in bis(2-methoxyethyl) ether at  $77^\circ\text{K}$  (the magnetic field is increasing from left to right)

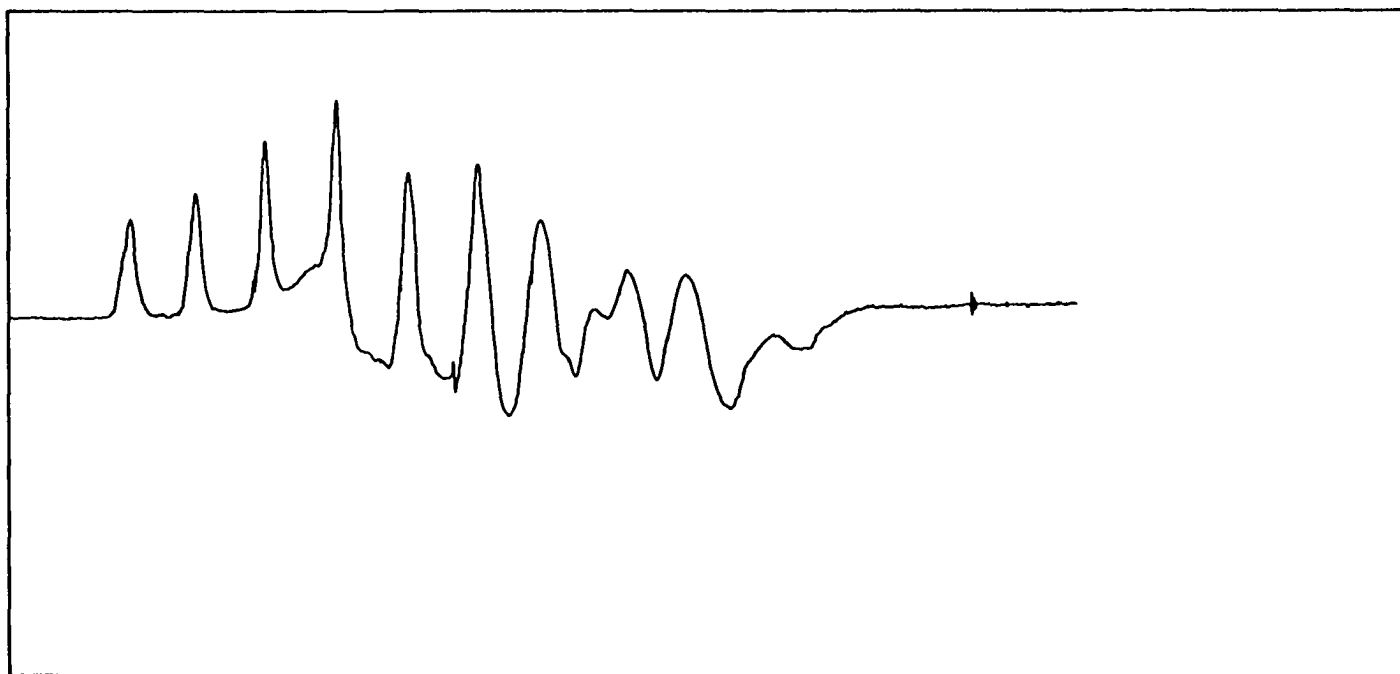


Fig. 17. EPR spectrum of  $\text{NbBr}_4$  in 2-methyl THF at  $77^\circ\text{K}$  (the magnetic field is increasing from left to right)

The concentration of the niobium(IV) complex was increased to 0.1 moles/liter in acetonitrile so that the "forbidden" d-d absorption band around  $19,000\text{ cm}^{-1}$  contributed to the recorded electronic spectrum. The spectra of dilute and concentrated solutions were resolved into Gaussian components by a computer program developed by the Ames Laboratory Computer Services Group. (A listing of the program is given in a Ph.D. thesis by Dr. J. L. Meyer, Iowa State University, Ames, Iowa, 1970). Wavelength and absorbance data from the experimental spectrum plus the number of components into which the spectrum should be resolved, estimated  $\epsilon_{\text{max}}$  (extinction coefficient at the absorption maximum), estimated  $\nu_0$  (wavenumber at the absorption maximum), and estimated half-width at half-height for each component were the input data needed to run the program. Data were derived for two peaks: one at  $\nu_0$  equal to  $25,500\text{ cm}^{-1}$  with  $\epsilon_{\text{max}}$  equal to 550 and the half-width at half-height equal to  $2362\text{ cm}^{-1}$ ; the other at  $\nu_0$  equal to  $19,550\text{ cm}^{-1}$  with  $\epsilon_{\text{max}}$  equal to 7 and the half-width at half-height equal to  $3480\text{ cm}^{-1}$ .<sup>1</sup> In Fig. 18 the maximum for what looks like a low

---

<sup>1</sup>The electronic spectrum showed no experimental evidence for a shoulder for an absorption peak at  $16,600\text{ cm}^{-1}$  assigned by Fowles, Tidmarsh, and Walton (33) to a d-d transition.

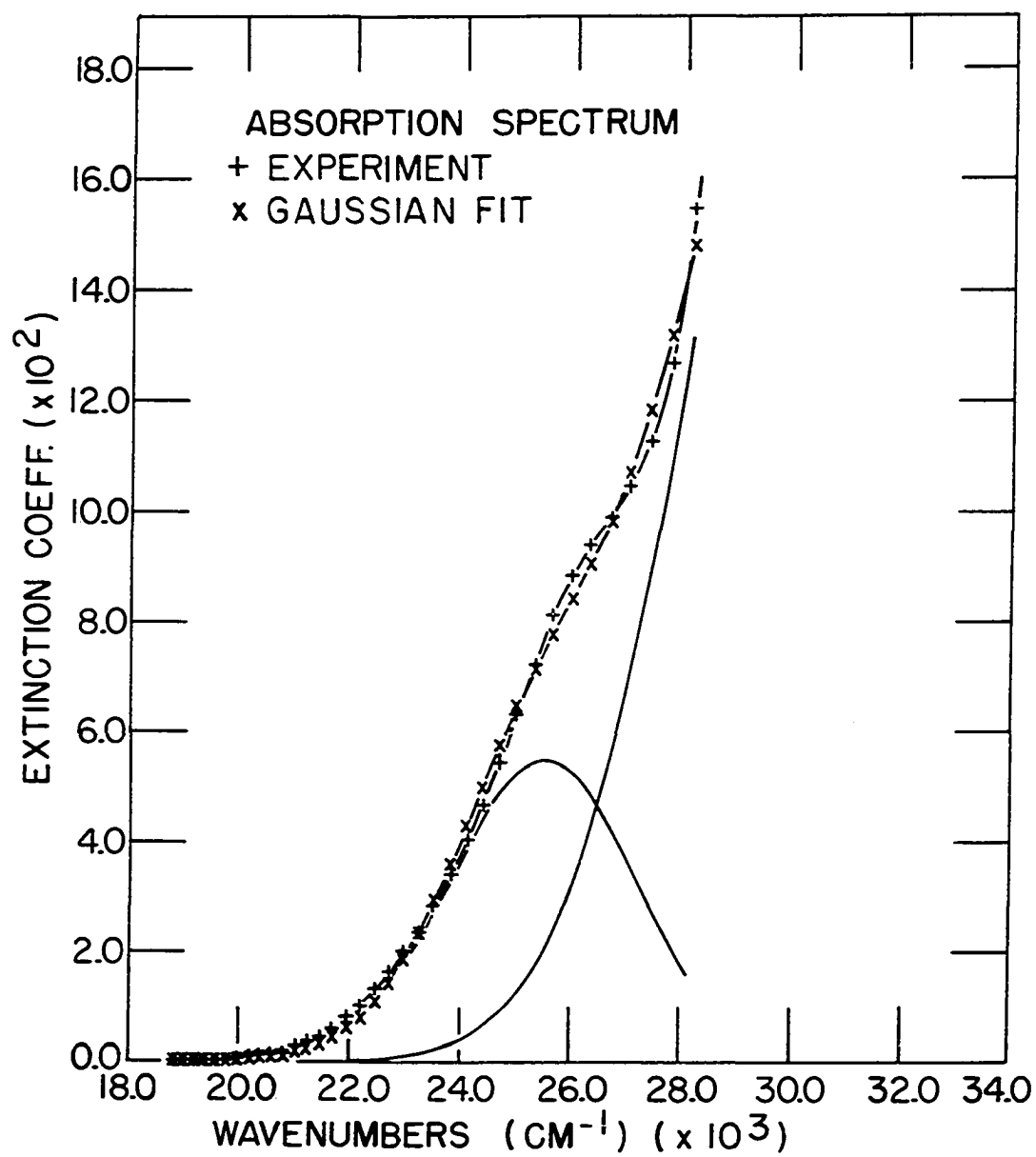


Fig. 18. Absorption spectrum for  $25,500 \text{ cm}^{-1}$  transition ( $\Delta_4$ ) of  $\text{NbBr}_4(\text{CH}_3\text{CN})_2$

intensity charge transfer band was assigned to a transition energy of  $25,500 \text{ cm}^{-1}$ . In Fig. 19, the maximum for the d-d band from the shoulder of the  $25,500 \text{ cm}^{-1}$  band was assigned a transition energy of  $19,550 \text{ cm}^{-1}$  above the ground state. The + sign represented values from the experimental spectrum and the X sign represented the sum of the Gaussian components. The experimental spectrum and sum of the Gaussian peaks agreed well within experimental error, i.e. within the uncertainty of the niobium concentration for the solutions.

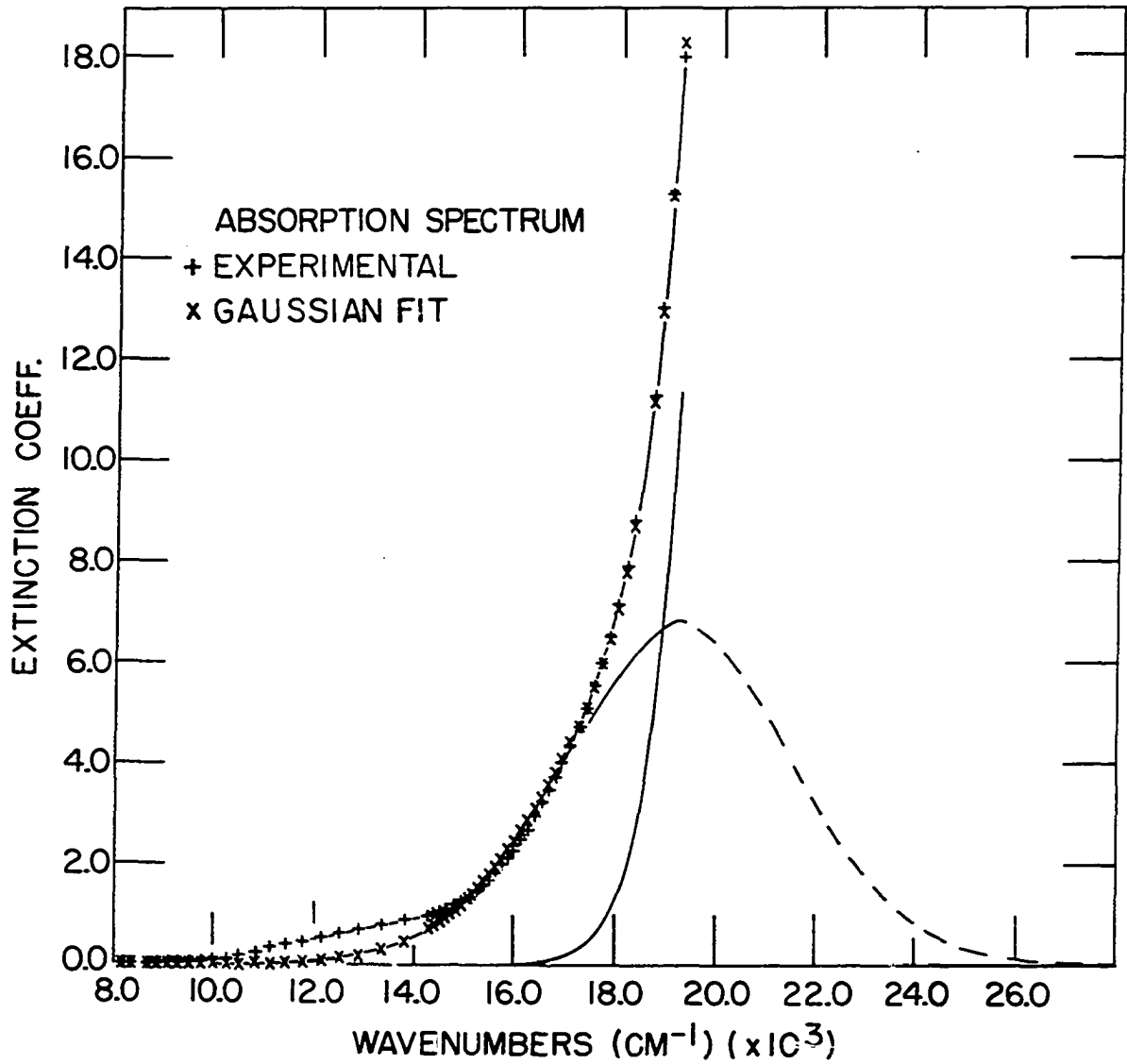


Fig. 19. Absorption spectrum for  $19,550 \text{ cm}^{-1}$  d-d transition ( $\Delta_3$ ) of  $\text{NbBr}_4(\text{CH}_3\text{CN})_2$

## RESULTS AND DISCUSSION

## Bonding

Experimental measurements of electronic d-d transitions and magnetic g-values were incorporated with theoretical crystal field wave functions in an attempt to semiempirically parameterize metal  $\sigma$  and  $\pi$  bonding in  $\text{NbBr}_4\text{Ac}_2$ . The substitution of acetonitrile ligands for two bromine atoms in cis positions caused reduction to  $C_{2v}$  point symmetry, split the  $T_{2g}$  and  $E_g$  states, and accounted for the large anisotropy in the g-values. The electronic d-d "forbidden" absorptions from the ground state to the excited  $T_{2g}$  and  $E_g$  states were no longer assigned to a single, unresolved, low intensity band from which the maximum absorption represented  $10 Dq$ . For  $\text{NbBr}_4\text{Ac}_2$  two of the four excited states were estimated to be  $4000 \text{ cm}^{-1}$  and  $19,550 \text{ cm}^{-1}$  above the ground state (p. 66). The first excited state was expected to be approximately  $2000 \text{ cm}^{-1}$  above the groundstate (p. 76) and the fourth excited state was expected to be hidden under the charge-transfer absorptions. The difference in the g-value from the spin-only, g equal to two, value was dependent upon the mixing of the ground state with excited states, but the magnitude of the difference in the g-value from the spin-only value, i.e.

the magnitude of the anisotropy, was dependent upon the magnitude of the transition energy from the ground state to the excited states. For a low symmetry complex, each anisotropic g-value expressed the interaction with different, non-degenerate excited states and, thus, separated the interactions in the sense that different wave functions corresponding to different excited states were predominately involved in a specific  $\sigma$  or  $\pi$  bond.

The octahedral wave functions were quantized along the  $C_2'$  axis so that these zero order wave functions were used as a basis to give reasonable g-value expressions containing first order energy terms. The problem was how to assign the d-d transition energies to correspond with the  $e_g$  and  $t_{2g}$  wave functions given in Table 2. For simplicity in notation the  $T_{2g}$  and  $E_g$  representations in octahedral symmetry (Table 2) were characterized by their representations when the symmetry descended from  $O_h$  to  $C_{2v}$ .

$$T_{2g}^a \rightarrow A_1' \quad (86)$$

$$T_{2g}^b \rightarrow B_1 \quad (87)$$

$$T_{2g}^c \rightarrow A_2 \quad (88)$$

$$E_g^a \rightarrow A_1'' \quad (89)$$

$$E_g^b \rightarrow B_2 \quad (90)$$



Referring to Fig. 1 the function  $B_2$  is similar to  $d_{yz}$  of the metal and bonds with the ligands in the  $y$ - $z$  plane, whereas, the function  $A_1''$  is a combination of  $d_{x^2-y^2}$  and  $d_{z^2}$  orbitals and bonds with the bromide ligands along the  $x$ -axis. For octahedral symmetry, the  $e_g$  orbitals are degenerate. Assuming the addition of acetonitrile lowers the energy level corresponding to the  $A_1''$  wave function and raises the energy level corresponding to the  $B_2$  wave function, then  $A_1''$  was assigned to the excited state  $19,550 \text{ cm}^{-1}$  above the ground state.

From Dougherty's crystal structure determination of  $\text{NbBr}_4\text{Ac}_2$  (2), the trans bromides and the niobium metal atom form a 160 degree angle in the  $x$ - $z$  molecular plane (Fig. 1). Here  $A_2$  (which resembles  $d_{xy}$ ) points farthest away from the ligands and was taken as the ground state. Positive evidence for  $A_2$  as the ground state was extracted from M.O. theory (pg 78) where  $A_2$  was the only orbital not allowed to participate in  $\sigma$ -bonding in the  $C_{2v}$  point group. Similarly,  $B_1$  (which looks like  $d_{xz}$ ) was assigned to the first excited state and  $A_1'$  (a combination of  $d_{z^2}$  and  $d_{x^2-y^2}$  which looks like " $d_{z^2-y^2}$ ") was assigned to the second excited state.

Substitution into the  $g_{zz}$ -value expression given by

Pryce (29) and discussed on page 34 gave:<sup>1</sup>

$$g_{zz} = 2 \left( 1 - \frac{3\lambda}{E(A_1'') - E(A_2)} - \frac{\lambda}{E(A_1') - E(A_2)} \right) \quad (91)$$

$$g_{zz} = 2 \left( 1 - \frac{3(750)}{19550} - \frac{750}{4000} \right) = 1.40$$

Substitution for  $E(B_2) - E(A_2)$  equal to  $25,500 \text{ cm}^{-1}$  gave:

$$g_{xx} = 2 \left( 1 - \frac{\lambda}{E(B_2) - E(A_2)} \right) = 2 \left( 1 - \frac{750}{25,500} \right) = 1.94 \quad (92)$$

Now the extinction coefficient for this band resolved in Fig. 18 was an order of magnitude larger than the extinction coefficient for the second and third excited states. If the band at  $25,500 \text{ cm}^{-1}$  was attributed to charge transfer, the fourth excited state probably was hidden under the charge transfer absorption peaks.

Substitution for  $g_{yy}$  equal to 1.30 gave  $E(B_1) - E(A_2)$ .

$$g_{yy} = 1.30 = 2 \left( 1 - \frac{\lambda}{E(B_1) - E(A_2)} \right) = 2 \left( 1 - \frac{750}{E(B_1) - E(A_2)} \right) \quad (93)$$

$$\Delta_1 = E(B_1) - E(A_2) \simeq 2100 \text{ cm}^{-1} \quad (94)$$

---

<sup>1</sup>For niobium(IV) the value of  $\lambda$ , the spin orbit coupling constant, was  $748 \text{ cm}^{-1}$ .

The transition  $\Delta_1$  to the first excited state was not observed experimentally. In the absorption spectra the ligand CN stretching band and Nujol absorption bands masked the forbidden d-d transition which was already expected to have a low extinction coefficient ( $\epsilon \lesssim 10$ ). Assuming tetragonal distortion, Torp (1) plotted  $\mu_{\text{eff}}$  vs.  $kT/\lambda$  and, by comparing plots made by Figgis (34) of  $\mu_{\text{eff}}$  versus  $kT/\lambda$  with different values of  $\Delta_1/\lambda$ , estimated  $\Delta_1$  to lie between 1000 and 2000  $\text{cm}^{-1}$ . From EPR measurements one observed directly the effect of the excited state,  $\Delta_1$  above the ground, on the g-tensor. The anisotropy in the  $g_{yy}$ -factor was caused by the interaction of the ground state with the first excited state (see Equation 93). Neglecting  $\pi$ -bonding for  $A_2$  and  $B_1$  functions,  $g_{yy}$  confirmed that the first excited state was significantly split from the ground state and from the second excited state.

The calculated value of  $g_{xx}$  agreed with the experimental value ( $1.95 \pm .06$ ) from single crystal work and with the value ( $1.91 \pm .03$ ) from  $\text{NbBr}_4\text{Ac}_2$  in the acetonitrile-toluene glass. Due to uncertainty in the assignment of the band at 25,500  $\text{cm}^{-1}$  and to the uncertainty in the g-value, this experimental and calculated agreement was still flexible enough to only tentatively assign the transition energy for the fourth

excited state.

The difference in experimental and calculated values of  $g_{zz}$  (i.e.  $\Delta g_{zz} = g_{zz}^{\text{exp}} - g_{zz}^{\text{cal}} = 0.35$ ) indicated that the zero order crystal field wave functions did not explain the EPR data. Pryce's theory (29) assumed  $\lambda$  was much smaller than  $\Delta_1$ , but correction terms, in our case, did not account for a difference of 0.35 in experimental and calculated g-values. For example if  $\lambda$  was less than  $\Delta_1$ ,  $g_{zz}$  calculated from the expression on page 36 given by Pake (30) was equal to 1.44. After reduction to the  $C_{2v}$  point symmetry, the excited states  $A_1''$  and  $A_1'$  can mix because of the addition of a low symmetry potential. Also, some mixing of ligand orbitals (LCAO-M.O.) with metal orbitals should form a more realistic bonding scheme. Incorporating molecular orbital theory and mixing excited states altered the g-value towards both the spin-only value and the experimental value.

The reducible representation for  $\sigma$ -bonding ( $C_{2v}$  point group) was:

$$(\sigma\text{-bonding}) = 3A_1 + B_1 + 2B_2 \quad (95)$$

The absence of  $A_2$ , the non-bonding representation, was in good agreement with the previous assignment of  $A_2$  as the ground state. In addition, the ground state  $A_2$  and the

excited states  $B_1$  and  $A_1'$  can all  $\pi$ -bond with the ligands, but from Dougherty's crystal structure determination (2),  $A_2$  points farthest away from the ligands, making  $\pi$ -bonding difficult. Again the ground state was taken as  $A_2$  without appreciable  $\pi$ -bonding. The expected M.O. and symmetry mixed wave functions are expressed in Equations 96 through 100. In these equations L represents the ligands and N represents the coefficient for the metal wave functions after normalization. The coefficients  $\alpha$  and  $\beta$  are needed to account for the mixing of  $A_1''$  and  $A_1'$ .

$$\psi_{\sigma_A}^* = N_{\sigma_A} (\alpha A_1'' + \beta A_1' - \gamma A_1^L(\sigma_A)) \quad (96)$$

$$\psi_{\sigma_B}^* = N_{\sigma_B} (B_2 - \gamma B_2^L) \quad (97)$$

$$\psi_{\pi_A}^* = N_{\pi_A} (\alpha A_1' + \beta A_1'' - \gamma A_1^L(\pi_A)) \quad (98)$$

$$\psi_{\pi_B}^* = N_{\pi_B} (B_1 - \gamma B_1^L) \quad (99)$$

$$\psi_{N.B.} = t_{2g}^c \quad (100)$$

The expressions for the g-values are expressed in Equations 101, 102 and 103. In these equations overlap was neglected and a correction for low-lying charge-transfer (C.T.) bands was included (7).

$$g_{xx} = 2 \left( 1 - \frac{N_{\sigma_B}^2 \lambda}{E(B_2) - E(A_2)} + \frac{(1 - N_{\sigma_B}^2) \lambda}{\Delta E(\text{C.T.})} \right) \quad (101)$$

$$g_{yy} = 2 \left( 1 - \frac{N_{\pi_B}^2 \lambda}{E(B_1) - E(A_2)} + \frac{(1 - N_{\pi_B}^2) \lambda}{\Delta E(\text{C.T.})} \right) \quad (102)$$

$$g_{zz} = 2 \left( 1 - \frac{(\alpha^2 + 2\sqrt{3\alpha\beta} + 3\beta^2) N_{\pi_A}^2 \lambda}{E(A_1') - E(A_2)} - \frac{(3\alpha^2 + 2\sqrt{3\alpha\beta} + \beta^2) N_{\sigma_A}^2 \lambda}{E(A_1'') - E(A_2)} \right. \\ \left. + \frac{(\alpha^2 + 2\sqrt{3\alpha\beta} + 3\beta^2) (1 - N_{\pi_A}^2) \lambda}{\Delta E(\text{C.T.})} + \frac{(3\alpha^2 + 2\sqrt{3\alpha\beta} + \beta^2) (1 - N_{\sigma_A}^2) \lambda}{\Delta E(\text{C.T.})} \right) \quad (103)$$

If no  $\pi$  or covalent bonding occurred, that is  $N_{\pi_A}^2$  equal to 1 and  $N_{\sigma_A}^2$  equal to 1, the experimental  $g_{zz}$  value may be explained from the application of low symmetry crystal field theory which requires mixing of the two  $A_1$  functions. If no mixing occurs  $g_{zz}$  still may be expressed in terms of two parameters  $N_{\pi_A}^2$  and  $N_{\sigma_A}^2$ . Torp (1) found that the C-N stretching frequency shifted to higher energies upon coordination indicating that little or no  $\pi$ -bonding took place from nitrile to metal. However, it is still possible that the metal orbital in the  $A_1'$  representation is released to  $\pi$ -bond with the bromides. The real situation probably consists of a combination of the mixing of excited states, some covalent bonding, and some  $\pi$ -bonding.

It was tempting to estimate values for  $N_{\pi_A}$  and  $N_{\sigma_A}$  (7) to quantitatively correlate  $g_{zz}$  calculated with  $g_{zz}$  observed. If  $\Delta_1$ , the energy separation for the first excited state, could be determined directly from the electronic spectra, one could predict the extent of  $\pi$ -bonding for the  $B_1$  representation. But, realistically, more experimental information is needed to adequately characterize the bonding in  $NbBr_4Ac_2$ .

### Magnetic Properties

The magnetic properties for complexes of the general formula  $NbX_4L_2$ , where X stands for halides and L stands for donor ligands, have not been well characterized from the magnetic susceptibility data. Fowles, Tidmarsh, and Walton (33) reported the effective magnetic moments obtained from the magnetic susceptibility data of a series of powdered  $MX_4L_2$  complexes at room temperature. Torp (1) also measured the effective magnetic moment from susceptibility data at temperatures ranging from 100°K to room temperature for powdered  $NbX_4L_2$ . The effective magnetic moments obtained by the two groups have been tabulated in Table 5 for  $NbBr_4Ac_2$  and  $NbCl_4Ac_2$  and compared with the magnetic moment calculated by substituting the average g-value obtained from the EPR powder spectrum of  $NbBr_4Ac_2$  and  $NbCl_4Ac_2$  into Equation 104.

$$\mu_{eff} = g(S(S+1))^{\frac{1}{2}} \quad (104)$$

Table 5. Effective magnetic moments from susceptibility and EPR measurements

Temp OK	$\mu_{\text{eff}}$ - NbBr <sub>4</sub> Ac <sub>2</sub>	$\mu_{\text{eff}}$ - NbCl <sub>4</sub> Ac <sub>2</sub>
300	1.57 (Torp)	1.82 (Torp)
293		1.55 (Fowles <u>et al.</u> )
291	1.34 (Fowles <u>et al.</u> )	
150	1.47 (Torp)	1.82 (Torp)
100	1.40 (Torp)	1.81 (Torp)
77	1.40 $\pm$ .03 (present EPR work)	1.47 (present EPR work)

The susceptibility data were inconclusive as to whether the complex had a cis or trans configuration.

If the complex was soluble in a glass, the EPR results gave a better test for determining cis or trans configurations from the line shape of the EPR spectrum. The EPR spectrum for trans complexes in a glass has two principal g-values; whereas the EPR spectrum for cis complexes has three principal g-values. In addition, information about the magnitude of the g-value anisotropy and about the coupling constants were estimated for NbBr<sub>4</sub>Ac<sub>2</sub> from the experimental and simulated spectra.

In conclusion, electron paramagnetic resonance spectroscopy seemed to be an excellent diagnostic tool for examining the magnetic properties of the MX<sub>4</sub>L<sub>2</sub> complexes having a d<sup>1</sup> configuration.



## BIBLIOGRAPHY

1. Torp, B. A., Spectra, magnetic susceptibilities and structure of some halogen complexes of niobium(IV) and tantalum(IV), Unpublished Ph.D. thesis, Ames, Iowa, Library, Iowa State University of Science and Technology, 1964.
2. Dougherty, T. A., The structure and infrared spectra of tetrahalobis(acetonitrile)niobium(IV) complexes, Unpublished Ph.D. thesis, Ames, Iowa, Library, Iowa State University of Science and Technology, 1964.
3. Fedotov, V. N., Garif'yanov, N. F., and Kozyrev, B. M., Dokl. Akad. Nauk SSSR 145, 1318 (1962).
4. Vinokurov, V. M., Zaripov, M. M., Stepanov, V. G., Chirkin, G. K., and Shekun, L. Ya., Soviet Phys.-Solid State 5, 1487 (1964).
5. Yafaev, N. R., and Garif'yanov, N. S., Soviet Phys.-Solid State 5, 2213 (1964).
6. Lardon, M. and Günthard, Hs. H., J. Chem. Phys. 44, 2010 (1966).
7. Rasmussen, P. G., Kuska, H. A., and Brubaker, C. H., Inorg. Chem. 4, 343 (1965).
8. Gainullin, I. F., Garif'yanov, N. S., and Kozyrev, B. M., Dokl. Akad. Nauk SSSR 180, 858 (1968).
9. Maniv, S., Low, W., Gabay, A., Phys. Lett. 29A, 536 (1969).
10. Mackay, R. A., and Schneider, R. F., Inorg. Chem. 6, 549 (1967).
11. Chester, P. F., J. Appl. Phys. 32, 866 (1961).
12. Chu, K. C., Kikuchi, C., and Viehmann, W., J. Chem. Phys. 46, 386 (1967).
13. Kikuchi, C. and Tseng, D. L., Bull. Amer. Phys. Soc. 14, 188 (1969).

14. Kim, Y. M., Reardon, D. E., and Bray, P. J., J. Chem. Phys. 48, 3396 (1968).
15. Edward, P. R., Subramanian, S., and Symons, M. C. R., J. Chem. Soc. A, 2985 (1968).
16. Breslow, R. A., Owens, F., and Gilliam, O. R., J. Chem. Phys. 53, 2143 (1970).
17. Bleaney, B., Bowers, K. D., and Pryce, M. W. L., Proc. Roy. Soc. (London) A228, 147 (1955).
18. Abragam, A. and Pryce, M. W. L., Proc. Roy. Soc. A205, 135 (1951).
19. Sroubek, Z. and Zdansky, K., J. Chem. Phys. 44, 3078 (1966).
20. Ballhausen, C. J., Introduction to ligand field theory, New York, New York, McGraw-Hill Book Co., Inc., 1962.
21. Gladney, H. M. and Swalen, J. D., J. Chem. Phys. 42, 1999 (1965).
22. Dionne, G. F., Phys. Rev. 137, A743 (1965).
23. McGarvey, B. R., Electron Spin Resonance of Transition Metal Complexes, in "Transition Metal Chemistry", R. L. Carlin, Ed., Marcel Dekker, Inc., New York, 1966, vol. 3, p. 160.
24. Hitchman, M. A., Olsen, C. D., Belford, R. L., J. Chem. Phys. 50, 1195 (1969).
25. Hitchman, M. A., Belford, R. L., Inorg. Chem. 8, 958 (1969).
26. Hitchman, M. A., Moores, B. W., and Belford, R. L., Inorg. Chem. 8, 1817 (1969).
27. Hitchman, M. A., J. Chem. Soc. A, 4 (1970).
28. Griffith, J. S., The theory of transition metal ions, London, England, Cambridge University Press, 1961.

29. Pryce, M. H. L., Proc. Phys. Soc. (London) A63, 25 (1950).
30. Pake, G. E., Paramagnetic Resonance, W. A. Benjamin, Inc., New York, 1962, pp. 55-62.
31. Okuda, T. and Date, M., J. Physical Soc. of Japan 28, 308 (1970).
32. Hitchman, M. A. and Belford, R. L., in "Electron Spin Resonance of Metal Complexes", T. F. Yen, Ed., Plenum Press, New York, N.Y., 1969, Chapter 7, p. 97.
33. Fowles, G. W. A., Tidmarsh, D. J., and Walton, R. A., Inorg. Chem. 8, 631 (1969).
34. Figgis, B. N., Trans. Faraday Soc. 57, 198 (1961).

## ACKNOWLEDGEMENTS

The author appreciates the opportunity provided by Prof. Robert E. McCarley to complete work on a thesis project which utilized EPR as a diagnostic tool. The author is very grateful to Dr. Robert E. McCarley for his patient guidance through the course of this work.

The author wishes to thank members of Physical and Inorganic Chemistry Group X for helpful discussions and good company.

Finally, the author wishes to thank his wife, Lynn for two sons, William and Thomas, who helped make the last two years in graduate school pass by quickly.